

# Statistical anisotropy in galaxy ellipticity correlations

Maresuke Shiraishi,<sup>a</sup> Teppei Okumura,<sup>b,c</sup> and Kazuyuki Akitsu<sup>d</sup>

<sup>a</sup>School of General and Management Studies, Suwa University of Science, Chino, Nagano 391-0292, Japan

<sup>b</sup>Academia Sinica Institute of Astronomy and Astrophysics (ASIAA), No. 1, Section 4, Roosevelt Road, Taipei 10617, Taiwan

<sup>c</sup>Kavli Institute for the Physics and Mathematics of the Universe (WPI), UTIAS, The University of Tokyo, Chiba 277-8583, Japan

<sup>d</sup>School of Natural Sciences, Institute for Advanced Study, 1 Einstein Drive, Princeton, NJ 08540, USA

E-mail: [shiraishi\\_maresuke@rs.sus.ac.jp](mailto:shiraishi_maresuke@rs.sus.ac.jp), [tokumura@asiaa.sinica.edu.tw](mailto:tokumura@asiaa.sinica.edu.tw), [kakitsu@ias.edu](mailto:kakitsu@ias.edu)

**Abstract.** As well as the galaxy number density and peculiar velocity, the galaxy intrinsic alignment can be used to test the cosmic isotropy. We study distinctive impacts of the isotropy breaking on the configuration-space two-point correlation functions (2PCFs) composed of the spin-2 galaxy ellipticity field. For this purpose, we build a methodology to efficiently compute general types of the isotropy-violating 2PCFs by generalizing the polypolar spherical harmonic decomposition approach to the spin-weighted version. As a demonstration, we analyze the 2PCFs when the matter power spectrum has a well-known  $g_*$ -type isotropy-breaking term (induced by, e.g., dark vector fields). We then confirm that some anisotropic distortions indeed appear in the 2PCFs and their shapes rely on a preferred direction causing the isotropy violation,  $\hat{d}$ . Such a feature can be a distinctive indicator for testing the cosmic isotropy. Comparing the isotropy-violating 2PCFs computed with and without the plane parallel (PP) approximation, we find that, depending on  $\hat{d}$ , the PP approximation is no longer valid when an opening angle between the directions towards target galaxies is  $\mathcal{O}(1^\circ)$  for the density-ellipticity and velocity-ellipticity cross correlations and around  $10^\circ$  for the ellipticity auto correlation. This suggests that an accurate test for the cosmic isotropy requires the formulation of the 2PCF without relying on the PP approximation.

---

## Contents

<b>1</b>	<b>Introduction</b>	<b>1</b>
<b>2</b>	<b>Preliminaries</b>	<b>2</b>
2.1	Spin-0 field: density $\delta$ and velocity $u$	2
2.2	Spin-2 field: ellipticity $\pm 2\gamma$	3
2.3	Unified form of the field	4
<b>3</b>	<b>Efficient computation methodology for general types of the isotropy-breaking correlations</b>	<b>4</b>
3.1	General types of the isotropy-breaking correlations	4
3.2	Spin-weighted tripolar spherical harmonic decomposition approach for the exact analysis	5
3.3	Spin-weighted bipolar spherical harmonic decomposition approach for the plane-parallel-limit analysis	6
<b>4</b>	<b>Correlations of the ellipticity field in the <math>g_*</math> model</b>	<b>8</b>
<b>5</b>	<b>Conclusions</b>	<b>12</b>
<b>A</b>	<b>Correlations of the density and velocity fields in the <math>g_*</math> model</b>	<b>14</b>
<b>B</b>	<b>Angular correlation functions</b>	<b>14</b>
<b>C</b>	<b>Useful mathematical identities</b>	<b>17</b>

---

## 1 Introduction

Global isotropy of the Universe is a major conjecture in cosmology, and it has been supported by various types of the cosmic observations so far. However, the possibility of a small isotropy violation still has been allowed and forthcoming observations will reveal it.

Theoretically, the statistical isotropy of the Universe can be violated by the existence of strong anisotropic sources like vector fields. There are already various inflationary scenarios including vector fields motivated by, e.g., magnetogenesis and axiverse models (see e.g. refs. [1–3] for review). Behaviors of vector fields as dark matter and dark energy candidates have also been thoroughly argued (e.g. refs. [4–7]). Testing the statistical isotropy in cosmic observables therefore becomes a powerful diagnostic approach of such scenarios. The cosmic microwave background (CMB) observations have already tightly constrained the statistical isotropy breaking [8–10], and a bit weaker limits have been obtained via the measurement of the galaxy number density from galaxy surveys [11, 12].

Regarding observables in the galaxy surveys, not only conventional spin-0 fields that are number density and peculiar velocity,<sup>1</sup> but also a spin-2 field, ellipticity, have rich information and hence the galaxy ellipticity field has recently come into use as a beneficial cosmological

---

<sup>1</sup>The peculiar velocity can also have a vorticity-induced spin-1 component, however, it is negligibly small in the standard cosmology.

probe (e.g. refs. [13–24]). Implementation of the ellipticity field in the isotropy test is naturally expected to improve the constraint or yield some novel information. Motivated by this, in this paper, we, for the first time, study distinctive impacts of the isotropy breaking on the configuration-space two-point correlation functions (2PCFs) composed of the ellipticity field.

The technique of spin-weighted polypolar spherical harmonic (PolypoSH) decomposition can be used as a powerful tool to compute galaxy statistics including the intricate spin and angular dependence.<sup>2</sup> Using this technique, previous studies presented the analysis of wide-angle effects of spin-0 [29–36] and higher-spin [37] field correlations, and isotropy-breaking signatures of spin-0 field ones [38–41]. We here generalize the decomposition technique to deal with general types of isotropy-breaking signatures on higher-spin field correlations.

As a numerical application of this new methodology, we analyze the 2PCFs generated in the case where the matter power spectrum has a well-known  $g_*$ -type isotropy-breaking term [11, 42] induced by, e.g., dark vector fields (hereinafter called the  $g_*$  model). For the first step, we examine the plane-parallel (PP) limit, where an opening angle (dubbed as  $\Theta$ ) between two line-of-sight (LOS) directions toward the positions of galaxies,  $\hat{x}_1 \equiv \mathbf{x}_1/x_1$  and  $\hat{x}_2 \equiv \mathbf{x}_2/x_2$ , is small enough that we can approximate  $\hat{x}_1 \simeq \hat{x}_2 = \hat{x}_p$ . Hence, the 2PCFs are computable using the spin-weighted bipolar spherical harmonic (BipoSH) basis,  $\{Y_\ell(\hat{x}_{12}) \otimes_{\lambda'} Y_{\ell'}(\hat{x}_p)\}_{LM}$ , where  $\hat{x}_{12} \equiv (\mathbf{x}_1 - \mathbf{x}_2)/|\mathbf{x}_1 - \mathbf{x}_2|$  is the direction of the separation vector between the positions of target galaxies. Showing obtained 2PCF signals as a function of parallel and perpendicular elements of  $\mathbf{x}_{12}$  as in ref. [43], we find some distinctive distortions due to the isotropy breaking, which could be a key indicator for testing the cosmic isotropy.

The PP approximation would not be applicable to the analysis in futuristic wider galaxy surveys. Therefore, as the next step, we treat  $\hat{x}_1$  and  $\hat{x}_2$  separately, and compute the 2PCFs by introducing the spin-weighted tripolar spherical harmonic (TripoSH) basis  $\{Y_\ell(\hat{x}_{12}) \otimes_{\lambda_1} Y_{\ell_1}(\hat{x}_1) \otimes_{\lambda_2} Y_{\ell_2}(\hat{x}_2)\}_{\ell' LM}$ . Comparing the exact results with the PP-limit ones for the  $g_*$  model, we measure the error level of the PP approximation as a function of  $\Theta$ . We then find that it is sensitive to a global preferred direction causing the isotropy violation and exceeds 10% up to  $\Theta = \mathcal{O}(1^\circ)$  at worst, indicating the importance of beyond the PP-limit analysis for testing the cosmic isotropy more accurately.

This paper is organized as follows. In the next section, we recall the linear theory formalism on the galaxy density, velocity and ellipticity fields. In section 3, we build an efficient computation methodology for general types of the isotropy-breaking 2PCFs with and without the PP approximation by means of the BipoSH and TripoSH techniques, respectively. Section 4 presents a numerical analysis of the 2PCFs in the  $g_*$  model, and the final section concludes this work.

## 2 Preliminaries

As our interests lie in large-scale statistics, throughout this paper, let us work with the linear theory expressions as follows.

### 2.1 Spin-0 field: density $\delta$ and velocity $u$

The number density fluctuation,  $\delta(\mathbf{x}) \equiv n(\mathbf{x})/\bar{n}(x) - 1$ , and the LOS component of peculiar velocity,  $u(\mathbf{x}) \equiv \mathbf{v}(\mathbf{x}) \cdot \hat{x}$ , are linearly connected to the real-space matter density contrast  $\delta_m$

---

<sup>2</sup>For different but similar approaches, see refs. [25–28].

as [31, 44]

$$\begin{aligned}\delta(\mathbf{x}) &= \int \frac{d^3k}{(2\pi)^3} e^{i\mathbf{k}\cdot\mathbf{x}} \left[ b_g - i \frac{\alpha f}{kx} (\hat{k} \cdot \hat{x}) + f (\hat{k} \cdot \hat{x})^2 \right] \delta_m(\mathbf{k}), \\ u(\mathbf{x}) &= \int \frac{d^3k}{(2\pi)^3} e^{i\mathbf{k}\cdot\mathbf{x}} i \frac{aHf}{k} (\hat{k} \cdot \hat{x}) \delta_m(\mathbf{k}),\end{aligned}\tag{2.1}$$

where  $b_g$  is the bias parameter for the density field,  $f$  is the linear growth rate,  $a$  is the scale factor,  $H$  is the Hubble parameter, and  $\alpha \equiv d \ln \bar{n}(x)/d \ln x + 2$  is the selection function of a given galaxy sample. Although these parameters and  $\delta_m$  depend on time, redshift or the comoving distance, it is not explicitly stated as an argument for notational convenience. This convention is adapted to all variables henceforth unless the parameter dependence is nontrivial and the explicit representation is needed. Note that eq. (2.1) corresponds to the redshift-space expression. The real-space one of the density field is simply obtained by taking the limit  $f \rightarrow 0$ . Regarding the velocity field, the real-space expression takes the same form as the redshift-space one at linear order [45].

## 2.2 Spin-2 field: ellipticity $\pm 2\gamma$

Similarly to the spin-0 case, the ellipticity field,  $\gamma_{ij}$ , the transverse and traceless projection of the second moment of the surface brightness of galaxies, is simply proportional to the real-space matter density contrast  $\delta_m$  under the linear alignment model [46, 47]

$$\begin{aligned}\gamma_{ij}(\mathbf{x}) &= \frac{1}{2} [P_{ik}(\hat{x})P_{jl}(\hat{x}) + P_{il}(\hat{x})P_{jk}(\hat{x}) - P_{ij}(\hat{x})P_{kl}(\hat{x})] \\ &\times \int \frac{d^3k}{(2\pi)^3} e^{i\mathbf{k}\cdot\mathbf{x}} \left( \hat{k}_k \hat{k}_l - \frac{1}{3} \delta_{kl}^K \right) b_K \delta_m(\mathbf{k}),\end{aligned}\tag{2.2}$$

where  $b_K$  is the bias parameter for the ellipticity field,  $\delta_{ij}^K$  denotes the Kronecker delta, and  $P_{ij}(\hat{x}) \equiv \delta_{ij}^K - \hat{x}_i \hat{x}_j$ . There is no distinction between the real and redshift space expressions at linear order. A conventionally-used  $+/ \times$  state is defined as

$$\begin{pmatrix} \gamma_+ \\ \gamma_\times \end{pmatrix}(\mathbf{x}) \equiv \begin{pmatrix} \hat{\theta}_i(\hat{x})\hat{\theta}_j(\hat{x}) - \hat{\phi}_i(\hat{x})\hat{\phi}_j(\hat{x}) \\ \hat{\theta}_i(\hat{x})\hat{\phi}_j(\hat{x}) + \hat{\phi}_i(\hat{x})\hat{\theta}_j(\hat{x}) \end{pmatrix} \gamma_{ij}(\mathbf{x}),\tag{2.3}$$

where  $\hat{x} \equiv (\sin \theta \cos \phi, \sin \theta \sin \phi, \cos \theta)$ ,  $\hat{\theta}(\hat{x}) \equiv (\cos \theta \cos \phi, \cos \theta \sin \phi, -\sin \theta)$  and  $\hat{\phi}(\hat{x}) \equiv (-\sin \phi, \cos \phi, 0)$  are three orthonormal vectors. Here, for good compatibility with the later PolypoSH decomposition, we also introduce a helicity  $\pm 2$  state as

$$\pm 2\gamma(\mathbf{x}) \equiv m_\mp^i(\hat{x})m_\mp^j(\hat{x})\gamma_{ij}(\mathbf{x}),\tag{2.4}$$

where the polarization vector, given by

$$\mathbf{m}_\pm(\hat{x}) \equiv \frac{1}{\sqrt{2}} \left[ \hat{\theta}(\hat{x}) \mp i\hat{\phi}(\hat{x}) \right],\tag{2.5}$$

obeys  $\hat{x} \cdot \mathbf{m}_\pm(\hat{x}) = 0$ ,  $\mathbf{m}_\pm^*(\hat{x}) = \mathbf{m}_\mp(\hat{x}) = \mathbf{m}_\pm(-\hat{x})$  and  $\mathbf{m}_\lambda(\hat{x}) \cdot \mathbf{m}_{\lambda'}(\hat{x}) = \delta_{\lambda, -\lambda'}^K$ . These two different states are linearly connected to each other and hence

$$\pm 2\gamma(\mathbf{x}) = \frac{1}{2} [\gamma_+(\mathbf{x}) \pm i\gamma_\times(\mathbf{x})].\tag{2.6}$$

Plugging eq. (2.2) into eq. (2.4), one can derive the linear-theory representation in the helicity state as

$$\pm 2\gamma(\mathbf{x}) = \int \frac{d^3k}{(2\pi)^3} e^{i\mathbf{k}\cdot\mathbf{x}} \hat{k}_i \hat{k}_j m_{\mp}^i(\hat{x}) m_{\mp}^j(\hat{x}) b_K \delta_{\mathbf{m}}(\mathbf{k}). \quad (2.7)$$

### 2.3 Unified form of the field

For later convenience, let us expand the above three fields (density, velocity and ellipticity) using the spin-weighted spherical harmonics as

$${}_{\lambda}X(\mathbf{x}) = \int \frac{d^3k}{(2\pi)^3} e^{i\mathbf{k}\cdot\mathbf{x}} \sum_{j\mu} \frac{4\pi c_j^X(k)}{2j+1} Y_{j\mu}(\hat{k}) {}_{-\lambda}Y_{j\mu}^*(\hat{x}) \delta_{\mathbf{m}}(\mathbf{k}), \quad (2.8)$$

where  $X = \{\delta, u, \gamma\}$  and

$$\begin{aligned} c_{\ell}^{\delta}(k) &= \left(b_g + \frac{1}{3}f\right) \delta_{\ell,0}^K - i \frac{\alpha f}{kx} \delta_{\ell,1}^K + \frac{2}{3}f \delta_{\ell,2}^K, \\ c_{\ell}^u(k) &= i \frac{aHf}{k} \delta_{\ell,1}^K, \\ c_{\ell}^{\gamma}(k) &= \frac{\sqrt{6}}{3} b_K \delta_{\ell,2}^K. \end{aligned} \quad (2.9)$$

The subscript  $\lambda$  in  ${}_{\lambda}X$  represents the spin/helicity dependence of each field; thus,  $\lambda = 0$  for  $X = \delta, u$ , and  $\lambda = \pm 2$  for  $X = \gamma$ . Regarding the spin-0 fields, for notational simplicity, we sometimes omit the subscript 0 in  ${}_0X$  as in eq. (2.1). To derive eq. (2.8), in the same manner as the CMB polyspectrum computations [48], we expand  $\hat{k}$ ,  $\hat{x}$ , and  $\mathbf{m}_{\pm}(\hat{x})$  in eqs. (2.1) and (2.7) with the spin-weighted spherical harmonics and simplify the products of them using the identities in appendix C. For  $\lambda = 0$ , eq. (2.8) recovers the usual Legendre expansion.

## 3 Efficient computation methodology for general types of the isotropy-breaking correlations

In this section, we shall build a computation methodology for the galaxy 2PCFs sourced from a general type of the isotropy-breaking matter power spectrum (3.2).

### 3.1 General types of the isotropy-breaking correlations

In the following analysis, we impose the statistical homogeneity of the matter fluctuation  $\delta_{\mathbf{m}}$ ; thus, the matter power spectrum generally takes the form

$$\langle \delta_{\mathbf{m}}(\mathbf{k}_1) \delta_{\mathbf{m}}(\mathbf{k}_2) \rangle = (2\pi)^3 \delta^{(3)}(\mathbf{k}_1 + \mathbf{k}_2) P_{\mathbf{m}}(\mathbf{k}_1). \quad (3.1)$$

As we are in position to consider the statistical isotropy violation of  $\delta_{\mathbf{m}}$ , the  $\hat{k}$  dependence remains in  $P_{\mathbf{m}}(\mathbf{k})$ . Without loss of generality, we can expand it according to

$$P_{\mathbf{m}}(\mathbf{k}) = \bar{P}_{\mathbf{m}}(k) \sum_{LM} G_{LM}(k) Y_{LM}(\hat{k}), \quad (3.2)$$

where  $G_{LM}^* = (-1)^M G_{L,-M}$  and  $G_{L=\text{odd},M} = 0$ . Breaking the statistical isotropy gives rise to nonvanishing  $G_{L>0,M}$ . On the other hand, we define  $G_{00} \equiv \sqrt{4\pi}$ , so that  $P_{\mathbf{m}}(\mathbf{k}) = \bar{P}_{\mathbf{m}}(k)$  holds if  $\delta_{\mathbf{m}}$  is statistically isotropic.

Computing the 2PCF of  ${}_{\lambda}X(\mathbf{x})$  by use of eqs. (2.8) and (3.1) and the addition theorem of the spherical harmonics (C.4) leads to

$$\begin{aligned}\xi_{\lambda_1\lambda_2}^{X_1X_2}(\mathbf{x}_{12}, \hat{x}_1, \hat{x}_2) &\equiv \langle {}_{\lambda_1}X_1(\mathbf{x}_1) {}_{\lambda_2}X_2(\mathbf{x}_2) \rangle \\ &= \int \frac{d^3k}{(2\pi)^3} e^{i\mathbf{k}\cdot\mathbf{x}_{12}} P_{\lambda_1\lambda_2}^{X_1X_2}(\mathbf{k}, \hat{x}_1, \hat{x}_2),\end{aligned}\quad (3.3)$$

where  $\mathbf{x}_{12} \equiv \mathbf{x}_1 - \mathbf{x}_2$  and

$$\begin{aligned}P_{\lambda_1\lambda_2}^{X_1X_2}(\mathbf{k}, \hat{x}_1, \hat{x}_2) &= \sum_{Jj_1j_2} \frac{(4\pi)^2 (-1)^{j_2} h_{Jj_1j_2}^{0\ 0\ 0}}{(2j_1+1)(2j_2+1)} c_{j_1}^{X_1}(k) c_{j_2}^{X_2}(k) \\ &\times \sum_{\mu\mu_1\mu_2} \begin{pmatrix} J & j_1 & j_2 \\ \mu & \mu_1 & \mu_2 \end{pmatrix} Y_{J\mu}^*(\hat{k}) {}_{-\lambda_1}Y_{j_1\mu_1}^*(\hat{x}_1) {}_{-\lambda_2}Y_{j_2\mu_2}^*(\hat{x}_2) P_m(\mathbf{k})\end{aligned}\quad (3.4)$$

with  $h_{l_1l_2l_3}^{s_1s_2s_3} \equiv \sqrt{\frac{(2l_1+1)(2l_2+1)(2l_3+1)}{4\pi}} \begin{pmatrix} l_1 & l_2 & l_3 \\ s_1 & s_2 & s_3 \end{pmatrix}$ . We note that  $P_{\lambda_1\lambda_2}^{X_1X_2}(\mathbf{k}, \hat{x}_1, \hat{x}_2)$  is not the Fourier counterpart of  $\xi_{\lambda_1\lambda_2}^{X_1X_2}(\mathbf{x}_{12}, \hat{x}_1, \hat{x}_2)$ .

If  $\hat{x}_1 = \hat{x}_2 \equiv \hat{x}_p$ , combining the spin-weighted spherical harmonics and reducing the Wigner symbols, one can further reduce eq. (3.4) to

$$\begin{aligned}P_{\lambda_1\lambda_2}^{X_1X_2}(\mathbf{k}, \hat{x}_p, \hat{x}_p) &= \sum_{Jj_1j_2} \frac{(4\pi)^2 (-1)^{j_2} h_{Jj_1j_2}^{0\ 0\ 0} h_J^{\lambda_1+\lambda_2\ -\lambda_1\ -\lambda_2}}{(2j_1+1)(2j_2+1)(2J+1)} c_{j_1}^{X_1}(k) c_{j_2}^{X_2}(k) \\ &\times \sum_{\mu} Y_{J\mu}^*(\hat{k})_{\lambda_1+\lambda_2} Y_{J\mu}(\hat{x}_p) P_m(\mathbf{k}).\end{aligned}\quad (3.5)$$

This corresponds to the expression used in the PP-limit analysis.

The relation between  $\xi_{\lambda_1\lambda_2}^{X_1X_2}$  and the angular correlation function defined on the celestial sphere  $\langle {}_{\lambda_1}a_{\ell_1m_1}^{X_1} {}_{\lambda_2}a_{\ell_2m_2}^{X_2} \rangle$  is summarized in appendix B.

### 3.2 Spin-weighted tripolar spherical harmonic decomposition approach for the exact analysis

As confirmed in refs. [12, 38, 40, 41], the PolypoSH decomposition approach is an efficient and fast way to compute the isotropy-breaking 2PCFs of the spin-0 fields such as the density  $\delta$  and the velocity  $u$ . We here generalize it to deal with the higher-spin fields as the ellipticity  $\pm 2\gamma$ . Our generalized formulae recover the 2PCFs obtained in ref. [37] at the isotropy-conserving limit.

Let us start from the computation without assuming the PP approximation. Since the 2PCF (3.3) is characterized by  $\hat{x}_{12}$ ,  $\hat{x}_1$  and  $\hat{x}_2$ , let us introduce a basis function of these three directions, i.e., the spin-weighted TripoSH:

$$\begin{aligned}{}_{\lambda_1\lambda_2}\mathcal{X}_{\ell\ell_1\ell_2\ell'}^{LM}(\hat{x}_{12}, \hat{x}_1, \hat{x}_2) &\equiv \{Y_{\ell}(\hat{x}_{12}) \otimes \{ {}_{\lambda_1}Y_{\ell_1}(\hat{x}_1) \otimes {}_{\lambda_2}Y_{\ell_2}(\hat{x}_2) \}_{\ell'}\}_{LM} \\ &= \sum_{mm_1m_2m'} \mathcal{C}_{\ell m \ell' m'}^{LM} \mathcal{C}_{\ell_1 m_1 \ell_2 m_2}^{\ell' m'} Y_{\ell m}(\hat{x}_{12}) {}_{\lambda_1}Y_{\ell_1 m_1}(\hat{x}_1) {}_{\lambda_2}Y_{\ell_2 m_2}(\hat{x}_2),\end{aligned}\quad (3.6)$$

and perform the following decomposition:

$$\xi_{\lambda_1\lambda_2}^{X_1X_2}(\mathbf{x}_{12}, \hat{x}_1, \hat{x}_2) = \sum_{\ell\ell_1\ell_2\ell'LM} {}_{\lambda_1\lambda_2}\Xi_{\ell\ell_1\ell_2\ell'}^{LMX_1X_2}(x_{12}) {}_{\lambda_1\lambda_2}\mathcal{X}_{\ell\ell_1\ell_2\ell'}^{LM}(\hat{x}_{12}, \hat{x}_1, \hat{x}_2),\quad (3.7)$$

where  $C_{l_1 m_1 l_2 m_2}^{l_3 m_3} \equiv (-1)^{l_1 - l_2 + m_3} \sqrt{2l_3 + 1} \begin{pmatrix} l_1 & l_2 & l_3 \\ m_1 & m_2 & -m_3 \end{pmatrix}$  is the Clebsch-Gordan coefficient.

To obtain the TripoSH coefficient  ${}_{\lambda_1 \lambda_2} \Xi_{\ell \ell_1 \ell_2 \ell'}^{LM X_1 X_2}$ , we also decompose  $P_{\lambda_1 \lambda_2}^{X_1 X_2}$  as

$$P_{\lambda_1 \lambda_2}^{X_1 X_2}(\mathbf{k}, \hat{x}_1, \hat{x}_2) = \sum_{\ell \ell_1 \ell_2 \ell' LM} {}_{\lambda_1 \lambda_2} \Pi_{\ell \ell_1 \ell_2 \ell'}^{LM X_1 X_2}(k) {}_{\lambda_1 \lambda_2} \mathcal{X}_{\ell \ell_1 \ell_2 \ell'}^{LM}(\hat{k}, \hat{x}_1, \hat{x}_2). \quad (3.8)$$

Substituting this into eq. (3.3), performing the  $\hat{k}$  integral by use of eq. (C.4), and comparing the resultant  $\xi_{\lambda_1 \lambda_2}^{X_1 X_2}$  with eq. (3.7), we derive the Hankel transformation rule:

$${}_{\lambda_1 \lambda_2} \Xi_{\ell \ell_1 \ell_2 \ell'}^{LM X_1 X_2}(x_{12}) = i^\ell \int_0^\infty \frac{k^2 dk}{2\pi^2} j_\ell(k x_{12}) {}_{\lambda_1 \lambda_2} \Pi_{\ell \ell_1 \ell_2 \ell'}^{LM X_1 X_2}(k). \quad (3.9)$$

This is computed after obtaining  ${}_{\lambda_1 \lambda_2} \Pi_{\ell \ell_1 \ell_2 \ell'}^{LM X_1 X_2}$  by use of

$${}_{\lambda_1 \lambda_2} \Pi_{\ell \ell_1 \ell_2 \ell'}^{LM X_1 X_2}(k) = \int d^2 \hat{k} \int d^2 \hat{x}_1 \int d^2 \hat{x}_2 P_{\lambda_1 \lambda_2}^{X_1 X_2}(\mathbf{k}, \hat{x}_1, \hat{x}_2) {}_{\lambda_1 \lambda_2} \mathcal{X}_{\ell \ell_1 \ell_2 \ell'}^{LM*}(\hat{k}, \hat{x}_1, \hat{x}_2). \quad (3.10)$$

Now, let us estimate  ${}_{\lambda_1 \lambda_2} \Pi_{\ell \ell_1 \ell_2 \ell'}^{LM X_1 X_2}$  from eqs. (3.2) and (3.4). Performing the spherical harmonic integrals and simplifying the resultant Wigner symbols by use of the identities in appendix C, we obtain

$${}_{\lambda_1 \lambda_2} \Pi_{\ell \ell_1 \ell_2 \ell'}^{LM X_1 X_2}(k) = \frac{(4\pi)^2 (-1)^{\lambda_1 + \lambda_2 + \ell_1 + L} h_{\ell_1 \ell_2 \ell'}^{0 \ 0 \ 0} h_{\ell \ell' L}^{000}}{(2\ell_1 + 1)(2\ell_2 + 1)\sqrt{2\ell' + 1}\sqrt{2L + 1}} c_{\ell_1}^{X_1}(k) c_{\ell_2}^{X_2}(k) \bar{P}_m(k) G_{LM}(k). \quad (3.11)$$

The number of nonvanishing multipoles is restricted by the selection rules:  $|\ell_1 - \ell_2| \leq \ell' \leq \ell_1 + \ell_2$ ,  $\ell_1 + \ell_2 + \ell' = \text{even}$ ,  $|\ell' - L| \leq \ell \leq \ell' + L$  and  $\ell + \ell' + L = \text{even}$ . From eq. (3.11), it is apparent that nonvanishing  $G_{LM}$  is linearly reflected on  ${}_{\lambda_1 \lambda_2} \Pi_{\ell \ell_1 \ell_2 \ell'}^{LM X_1 X_2}$ . Note that  ${}_{\lambda_1 \lambda_2} \Pi_{\ell \ell_1 \ell_2 \ell'}^{00 X_1 X_2}$  or  ${}_{\lambda_1 \lambda_2} \Xi_{\ell \ell_1 \ell_2 \ell'}^{00 X_1 X_2}$  completely recovers the TripoSH coefficient computed from the isotropy-conserving matter power spectrum in ref. [37] because of  $h_{\ell \ell' 0}^{000} = (-1)^\ell \sqrt{\frac{2\ell+1}{4\pi}} \delta_{\ell \ell'}^K$ .

Figure 1 depicts all nonvanishing  $L = 2$  TripoSH coefficients of the  $\delta\gamma$ ,  $u\gamma$  and  $\gamma\gamma$  correlations as a function of  $x_{12}$ . Here we assume  $G_{LM} \propto k^0$ , so that  $G_{LM}$  can be singled out in the TripoSH coefficient as  ${}_{\lambda_1 \lambda_2} \Xi_{\ell \ell_1 \ell_2 \ell'}^{LM X_1 X_2} = \frac{G_{LM}}{\sqrt{4\pi}} {}_{\lambda_1 \lambda_2} \Xi_{\ell \ell_1 \ell_2 \ell'}^{L X_1 X_2}$ . This figure rather shows the reduced coefficient  ${}_{\lambda_1 \lambda_2} \Xi_{\ell \ell_1 \ell_2 \ell'}^{2 X_1 X_2}$ . At each multipole, the baryon acoustic oscillation (BAO) bump at  $x_{12} \simeq 100h^{-1}$  Mpc is confirmed. It is also apparent that the redshift-space distortion (RSD) effect induces higher multipoles in the  $\delta\gamma$  correlation, making the difference in shape between the real and redshift space 2PCFs as seen in section 4 and appendix A.

The results in figure 1 are utilized for computing the 2PCFs of the  $g_*$  model in section 4.

### 3.3 Spin-weighted bipolar spherical harmonic decomposition approach for the plane-parallel-limit analysis

In the following, we reduce the above expression to that in the PP limit. In this limit, the 2PCF is characterized by  $\hat{x}_{12}$  and  $\hat{x}_p$  that is a LOS direction chosen as satisfying  $\hat{x}_p \simeq \hat{x}_1 \simeq \hat{x}_2$ ; therefore, the decomposition formula reduces to

$$\begin{aligned} \xi_{\lambda_1 \lambda_2 \text{PP}}^{X_1 X_2}(\mathbf{x}_{12}, \hat{x}_p) &\equiv \xi_{\lambda_1 \lambda_2}^{X_1 X_2}(\mathbf{x}_{12}, \hat{x}_p, \hat{x}_p) \\ &= \sum_{\ell' LM} {}_{\lambda_1 \lambda_2} \xi_{\ell \ell'}^{LM X_1 X_2}(x_{12}) {}_{\lambda_1 + \lambda_2} X_{\ell \ell'}^{LM}(\hat{x}_{12}, \hat{x}_p), \end{aligned} \quad (3.12)$$

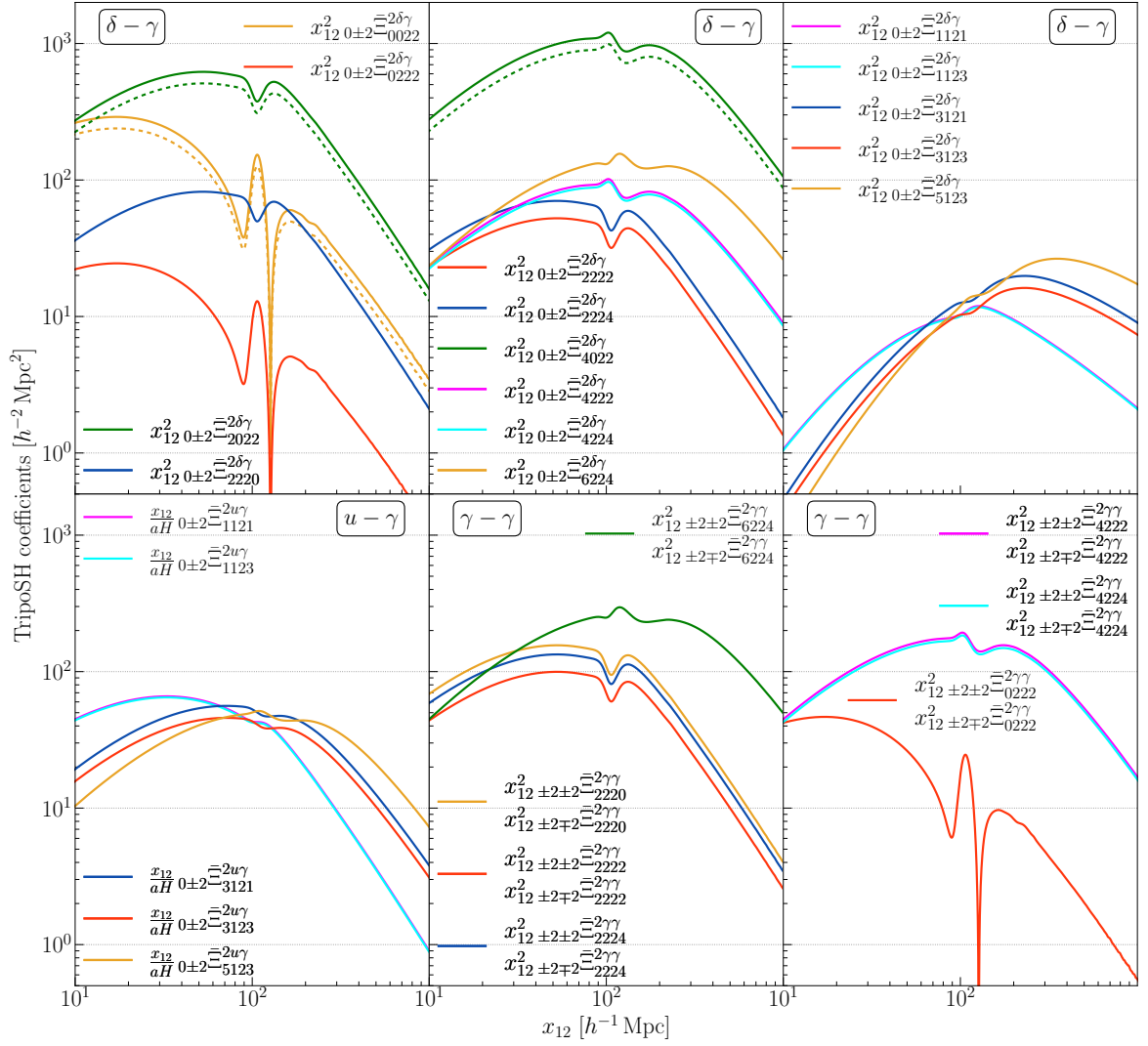


**Figure 1.** Absolute values of all reduced TripoSH coefficients for  $L = 2$ :  $0\pm 2\Xi_{\ell\ell_1\ell_2\ell'}^{2\delta\gamma}$  (top three panels),  $0\pm 2\Xi_{\ell\ell_1\ell_2\ell'}^{2u\gamma}$  (bottom left panel) and  $\pm 2\pm 2\Xi_{\ell\ell_1\ell_2\ell'}^{2\gamma\gamma} = \pm 2\mp 2\Xi_{\ell\ell_1\ell_2\ell'}^{2\gamma\gamma}$  (bottom center and right panels) as a function of  $x_{12}$  for  $z_1 = z_2 = 0.3$  and  $b_g = b_K = 1$ . Solid and dashed lines discriminate between the results in the redshift and real spaces, respectively. Note that the reduced TripoSH coefficient  $\lambda_1\lambda_2\Xi_{\ell\ell_1\ell_2\ell'}^{LX_1X_2}$  is defined as the original TripoSH one  $\lambda_1\lambda_2\Xi_{\ell\ell_1\ell_2\ell'}^{LMX_1X_2}$  divided by  $G_{LM}$  when  $G_{LM} \propto k^0$  and therefore independent of  $G_{LM}$ .

where the spin-weighted Biposh basis is defined as

$$\begin{aligned} \lambda' X_{\ell\ell'}^{LM}(\hat{x}_{12}, \hat{x}_p) &\equiv \{Y_\ell(\hat{x}_{12}) \otimes \lambda' Y_{\ell'}(\hat{x}_p)\}_{LM} \\ &= \sum_{mm'} \mathcal{C}_{\ell m \ell' m'}^{LM} Y_{\ell m}(\hat{x}_{12}) \lambda' Y_{\ell' m'}(\hat{x}_p). \end{aligned} \quad (3.13)$$

In a similar manner to the TripoSH decomposition, we perform the Fourier-space pre-



decomposition:

$$\begin{aligned} P_{\lambda_1 \lambda_2 \text{PP}}^{X_1 X_2}(\mathbf{k}, \hat{x}_p) &\equiv P_{\lambda_1 \lambda_2}^{X_1 X_2}(\mathbf{k}, \hat{x}_p, \hat{x}_p) \\ &= \sum_{\ell \ell' LM} \lambda_1 \lambda_2 \pi_{\ell \ell'}^{LM X_1 X_2}(k)_{\lambda_1 + \lambda_2} X_{\ell \ell'}^{LM}(\hat{k}, \hat{x}_p). \end{aligned} \quad (3.14)$$

With this, eqs. (3.3), (3.12) and the identities in appendix C, we derive the Hankel transformation formula:

$$\lambda_1 \lambda_2 \xi_{\ell \ell'}^{LM X_1 X_2}(x_{12}) = i^\ell \int_0^\infty \frac{k^2 dk}{2\pi^2} j_\ell(k x_{12})_{\lambda_1 \lambda_2} \pi_{\ell \ell'}^{LM X_1 X_2}(k), \quad (3.15)$$

where

$$\lambda_1 \lambda_2 \pi_{\ell \ell'}^{LM X_1 X_2}(k) = \int d^2 \hat{k} \int d^2 \hat{x}_p P_{\lambda_1 \lambda_2 \text{PP}}^{X_1 X_2}(\mathbf{k}, \hat{x}_p)_{\lambda_1 + \lambda_2} X_{\ell \ell'}^{LM*}(\hat{k}, \hat{x}_p). \quad (3.16)$$

Because of the relation between the TripoSH and BipoSH bases:

$$\lambda_1 \lambda_2 \mathcal{X}_{\ell_1 \ell_2 \ell'}^{LM}(\hat{x}_{12}, \hat{x}_p, \hat{x}_p) = (-1)^{\ell_1 - \ell_2 + \lambda_1 + \lambda_2} \frac{h_{\ell_1}^{-\lambda_1} h_{\ell_2}^{-\lambda_2} h_{\ell'}^{\lambda_1 + \lambda_2}}{\sqrt{2\ell' + 1}} \lambda_1 \lambda_2 X_{\ell \ell'}^{LM}(\hat{x}_{12}, \hat{x}_p), \quad (3.17)$$

the BipoSH coefficients can directly be inverted from the TripoSH ones as

$$\begin{aligned} \lambda_1 \lambda_2 \xi_{\ell \ell'}^{LM X_1 X_2}(x_{12}) &= \sum_{\ell_1 \ell_2} (-1)^{\ell_1 - \ell_2 + \lambda_1 + \lambda_2} \frac{h_{\ell_1}^{-\lambda_1} h_{\ell_2}^{-\lambda_2} h_{\ell'}^{\lambda_1 + \lambda_2}}{\sqrt{2\ell' + 1}} \lambda_1 \lambda_2 \Xi_{\ell \ell_1 \ell_2 \ell'}^{LM X_1 X_2}(x_{12}), \\ \lambda_1 \lambda_2 \pi_{\ell \ell'}^{LM X_1 X_2}(k) &= \sum_{\ell_1 \ell_2} (-1)^{\ell_1 - \ell_2 + \lambda_1 + \lambda_2} \frac{h_{\ell_1}^{-\lambda_1} h_{\ell_2}^{-\lambda_2} h_{\ell'}^{\lambda_1 + \lambda_2}}{\sqrt{2\ell' + 1}} \lambda_1 \lambda_2 \Pi_{\ell \ell_1 \ell_2 \ell'}^{LM X_1 X_2}(k). \end{aligned} \quad (3.18)$$

Plugging eqs. (3.2) and (3.5) into eq. (3.16) and simplifying the integrals, or more simply, computing eq. (3.18) with eq. (3.11), we obtain

$$\lambda_1 \lambda_2 \pi_{\ell \ell'}^{LM X_1 X_2}(k) = \sum_{\ell_1 \ell_2} \frac{(4\pi)^2 (-1)^{\ell_2 + L} h_{\ell_1}^{-\lambda_1} h_{\ell_2}^{-\lambda_2} h_{\ell'}^{\lambda_1 + \lambda_2} h_{\ell_1 \ell_2 \ell'}^0 h_{\ell \ell' L}^{000}}{(2\ell_1 + 1)(2\ell_2 + 1)(2\ell' + 1)\sqrt{2L + 1}} c_{\ell_1}^{X_1}(k) c_{\ell_2}^{X_2}(k) \bar{P}_m(k) G_{LM}(k). \quad (3.19)$$

The isotropy-conserving matter power spectrum induces only  $\lambda_1 \lambda_2 \pi_{\ell \ell'}^{00 X_1 X_2}$  or  $\lambda_1 \lambda_2 \xi_{\ell \ell'}^{00 X_1 X_2}$ . The 2PCFs computed from these fully recover the results in ref. [43]<sup>3</sup>

#### 4 Correlations of the ellipticity field in the $g_*$ model

Now we move to the numerical computation of the 2PCFs for a concrete scenario where the matter power spectrum includes a scale-invariant isotropy-breaking term whose magnitude is parametrized by  $g_*$ , reading

$$\begin{aligned} P_m(\mathbf{k}) &= \bar{P}_m(k) \left[ 1 + g_* \left\{ (\hat{k} \cdot \hat{d})^2 - \frac{1}{3} \right\} \right] \\ &= \bar{P}_m(k) \left[ \mathcal{L}_0(\hat{k} \cdot \hat{d}) + \frac{2}{3} g_* \mathcal{L}_2(\hat{k} \cdot \hat{d}) \right], \end{aligned} \quad (4.1)$$

<sup>3</sup>The 2PCFs computed in ref. [43],  $\xi_{g+}$ ,  $\xi_{v+}$  and  $\xi_{\pm}$ , are related to ours according to  $\xi_{g+} = \xi_{0+2}^{\delta\gamma} + \xi_{0-2}^{\delta\gamma}$ ,  $\xi_{v+} = \xi_{0+2}^{u\gamma} + \xi_{0-2}^{u\gamma}$  and  $\xi_{\pm} = 2(\xi_{+2\mp 2}^{\gamma\gamma} + \xi_{-2\pm 2}^{\gamma\gamma})$ .

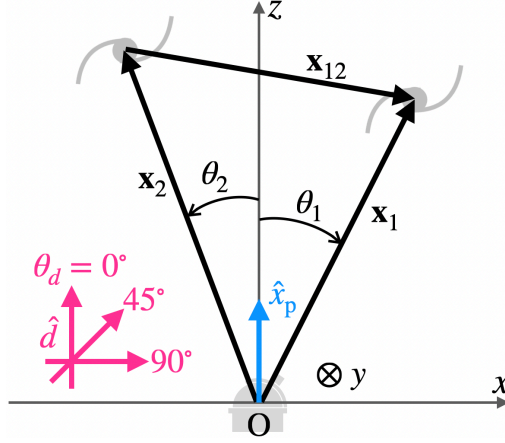


**Figure 2.** Coordinate system adopted in the computation of the 2PCFs using the exact form  $\xi_{\lambda_1 \lambda_2}^{X_1 X_2}(\mathbf{x}_{12}, \hat{x}_1, \hat{x}_2)$  and the PP approximation  $\xi_{\lambda_1 \lambda_2}^{X_1 X_2 \text{PP}}(\mathbf{x}_{12}, \hat{x}_p)$ .

where  $\hat{d}$  denotes some global preferred direction, and  $\mathcal{L}_\ell(x)$  is the Legendre polynomial. With eq. (C.1), one can find the form of  $G_{LM}$  in eq. (3.2) as

$$G_{LM} = \sqrt{4\pi} \delta_{L,0}^K \delta_{M,0}^K + \frac{8\pi}{15} g_* Y_{2M}^*(\hat{d}) \delta_{L,2}^K. \quad (4.2)$$

As confirmed in the previous section, the former ( $G_{00}$ ) and latter ( $G_{2M}$ ) terms make nonvanishing TripoSH coefficients  ${}_{\lambda_1 \lambda_2} \Xi_{\ell \ell_1 \ell_2 \ell'}^{00 X_1 X_2}$  and  ${}_{\lambda_1 \lambda_2} \Xi_{\ell \ell_1 \ell_2 \ell'}^{2M X_1 X_2}$ , respectively. For late convenience, let us notationally differentiate the 2PCF to two terms as

$$\xi_{\lambda_1 \lambda_2}^{X_1 X_2} = {}^{(0)}\xi_{\lambda_1 \lambda_2}^{X_1 X_2} + g_* {}^{(2)}\xi_{\lambda_1 \lambda_2}^{X_1 X_2}. \quad (4.3)$$

The former and latter terms correspond to the isotropy-conserving and isotropy-breaking parts, respectively.

The matter power spectrum (3.2) for  $G_{L>0,M} \neq 0$  can be generated by the existence of some anisotropic source. If there are (spin-1) vector fields which couple to inflaton or non-inflaton scalar ones in the inflationary era, nonvanishing  $g_*$  or  $G_{2M}$  arises as well as  $G_{00}$  (e.g., refs. [49–56]). In more general, spin- $s$  fields produce nonzero  $G_{00}$ ,  $G_{2M}$ ,  $G_{4M}$ ,  $\dots$ ,  $G_{2(s-1),M}$  and  $G_{2s,M}$  [39, 57]. Other kinds of sources, e.g., two-form fields [58], an inflating solid or elastic medium [59, 60], fossil gravitational waves [61–64] and large scale tides beyond the survey region [40, 65–68] also induce nonvanishing  $G_{L>0,M}$ . The spectral shape of the induced  $G_{LM}$  relies on the choice of, e.g., the coupling function and the potential of the fields. In the following 2PCF computations, let us focus on the simplest case where  $g_*$  becomes constant in wavenumber. By the recent analysis with the CMB [8] and galaxy density fields [12],  $g_* > \mathcal{O}(10^{-2})$  is disfavored.

To make our discussion simpler, we shall work on the coordinate system where the three direction vectors  $\hat{x}_{12}$ ,  $\hat{x}_1$  and  $\hat{x}_2$  are on the  $xz$  plane and parametrized as  $\hat{x}_{12} = (\sin \theta_{12}, 0, \cos \theta_{12})$ ,  $\hat{x}_1 = (\sin \theta_1, 0, \cos \theta_1)$  and  $\hat{x}_2 = (-\sin \theta_2, 0, \cos \theta_2)$  (here, the polar angles are fixed as  $\phi_{12} = \phi_1 = 0$  and  $\phi_2 = \pi$ ). In the PP limit; namely,  $\theta_1 \rightarrow 0$  and  $\theta_2 \rightarrow 0$ , the two different LOS directions  $\hat{x}_1$  and  $\hat{x}_2$  can be identified with the  $z$ -axis positive direction, so that  $\hat{x}_p = (0, 0, 1)$ . In the following, we examine how the 2PCFs are distorted depending

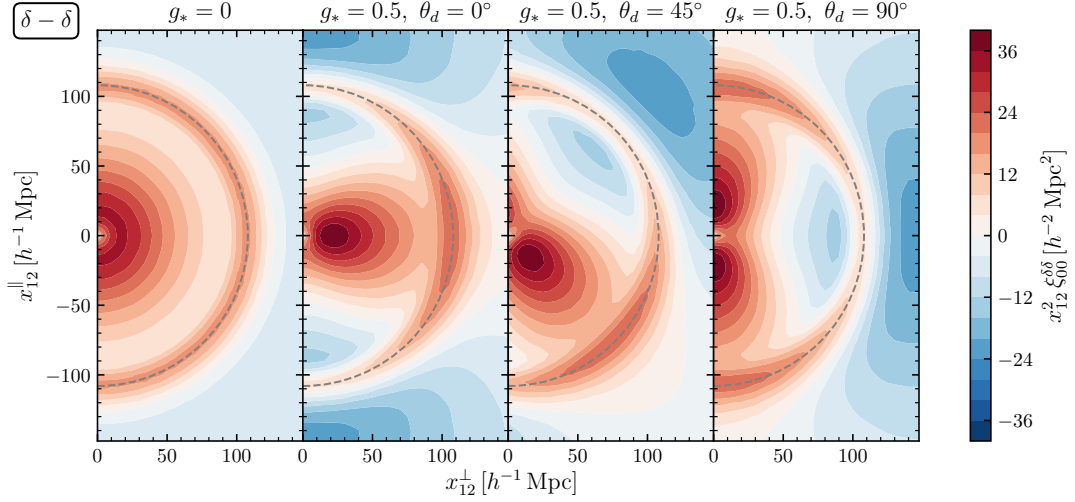


**Figure 3.** Intensity distributions of the real-space  $\delta\delta$  correlation in the PP limit on the  $(x_{12}^{\perp}, x_{12}^{\parallel})$  plane for  $z_1 = z_2 = 0.3$  and  $b_g = b_K = 1$ . The leftmost and the other three right panels show the results for  $g_* = 0$  and  $0.5$ , respectively (we consider such a large  $g_*$  to highlight the isotropy-breaking signatures although it is disfavored by observations). For the latter, three different  $\hat{d}$ :  $\theta_d = 0^\circ$ ,  $45^\circ$  and  $90^\circ$  are considered. The region for  $x_{12}^{\perp} \geq 0$  is only shown, while one can reconstruct the region for  $x_{12}^{\perp} < 0$  as these 2PCFs are symmetric or antisymmetric with respect to the origin. For reference, the BAO scale,  $x_{12} \simeq 100h^{-1}$  Mpc, is displayed with the dashed gray circles.

on the preferred direction  $\hat{d} = (\sin\theta_d \cos\phi_d, \sin\theta_d \sin\phi_d, \cos\theta_d)$  by considering three different cases:  $\theta_d = 0^\circ$ ,  $45^\circ$  and  $90^\circ$  with  $\phi_d = 0$ , equivalently,  $\hat{d} = (0, 0, 1)$ ,  $(\frac{1}{\sqrt{2}}, 0, \frac{1}{\sqrt{2}})$  and  $(1, 0, 0)$ . For  $\theta_d = 0^\circ$  and  $90^\circ$ ,  $\hat{d} = \hat{x}_p$  and  $\hat{d} \perp \hat{x}_p$  hold, respectively. Even investigating  $90^\circ \leq \theta_d \leq 180^\circ$ , the symmetric results are obtained. Moreover, the distortion shapes depend weakly on the  $y$ -axis component of  $\hat{d}$ , so that we do not pick up any other  $\hat{d}$ . The coordinate system and settings mentioned above are visually summarized in figure 2.

We shall first assess the shape change of the 2PCFs depending on  $\hat{d}$  based on the PP-limit results. For this purpose, we analyze  $\xi_{\lambda_1\lambda_2}^{X_1X_2}(\mathbf{x}_{12}, \hat{x}_p)$  as a function of  $x_{12}^{\perp}$  and  $x_{12}^{\parallel}$ , the components of  $\mathbf{x}_{12}$  perpendicular and parallel to the LOS direction  $\hat{x}_p$ . In the computation, we set  $\mathbf{x}_{12} = (x_{12}^{\perp}, 0, x_{12}^{\parallel})$  and thus adopt  $\theta_{12} = \arccos(\hat{x}_{12} \cdot \hat{x}_p) = \arccos(x_{12}^{\parallel}/x_{12})$  and  $x_{12} = \sqrt{(x_{12}^{\parallel})^2 + (x_{12}^{\perp})^2}$ . Figures 3, 4, 5 and 7 depict the results for several  $g_*$  and  $\theta_d$ .

Here, let us begin with the assessment of the  $\delta\delta$  correlations in the real space as the isotropy-breaking signatures are most clearly apparent there. From figure 3, one can easily find that nonzero  $g_*$  distorts the 2PCF depending on  $\theta_d$ . For  $\theta_d = 0^\circ$ , since  $\hat{x}_p = \hat{d}$ , the 2PCF is distorted along the  $x_{12}^{\perp}$  axis. This looks similar to the RSD effect in the redshift-space  $\delta\delta$  correlation (top leftmost panel in figure 7). On the other hand, for  $\theta_d = 90^\circ$  and  $45^\circ$ , the distortions seem to appear in a direction along the  $x_{12}^{\parallel}$  axis and the diagonal line, respectively. Such a feature could be a distinctive indicator for testing the cosmic isotropy. For the other types of the 2PCFs described in figures 4, 5 and 7, the isotropy-breaking signatures due to nonzero  $g_*$  are sometimes degenerate with the isotropy-conserving ones when  $g_* = 0$ , and the above trend is then slightly perceptible.

We further go through the 2PCF beyond the PP limit by use of the TripoSH decompo-

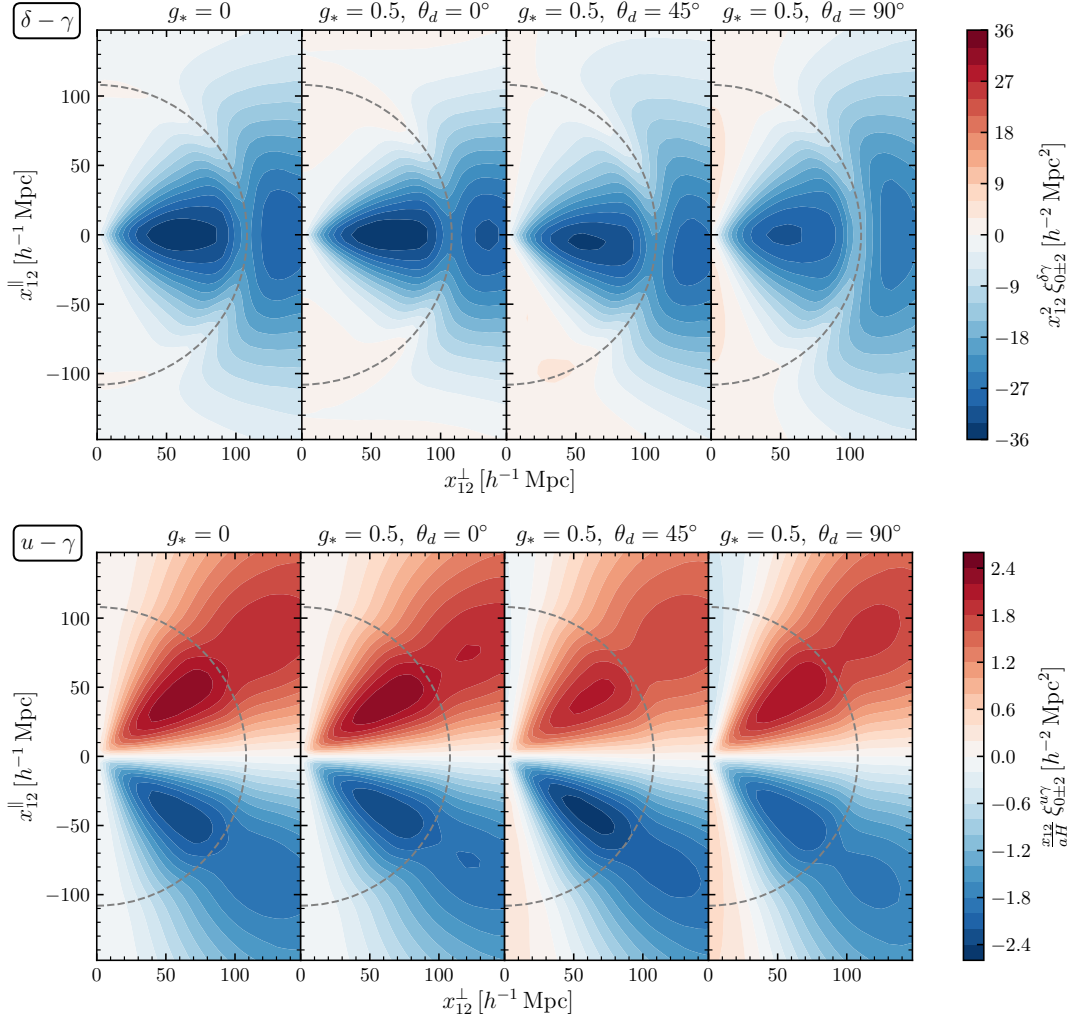


**Figure 4.** Same as figure 3, except for the  $\delta\gamma$  correlation in the redshift space and the  $u\gamma$  correlation.

sition technique. For numerical computations of  $\xi_{\lambda_1\lambda_2}^{X_1X_2}(\mathbf{x}_{12}, \hat{x}_1, \hat{x}_2)$ , we impose  $\hat{x}_{12} = (1, 0, 0)$  (i.e.,  $\theta_{12} = 90^\circ$ ) and  $\theta_1 = \theta_2$  and define the opening angle between  $\hat{x}_1$  and  $\hat{x}_2$  as  $\Theta \equiv \theta_1 + \theta_2 = 2\theta_1 = 2\theta_2$ . Due to these conditions, a triangle formed by  $\mathbf{x}_{12}$ ,  $\mathbf{x}_1$  and  $\mathbf{x}_2$  becomes isosceles.

The results of the  $\delta\gamma$ ,  $u\gamma$  and  $\gamma\gamma$  correlations including nonzero  $g_*$  at several  $x_{12}$  or  $\Theta$  are summarized in figure 6. One can confirm from this that the distortion level of the 2PCF for a certain  $g_*$  changes depending on  $\theta_d$ . It is enhanced as  $\theta_d$  increases for the  $\delta\gamma$  or  $\gamma\gamma$  case, while maximized at  $\theta_d \sim 45^\circ$  for the  $u\gamma$  one (see the top panels). The latter feature is confirmed also from the  $\delta u$  correlations (see figure 8).

From figure 6, one can also study how accurate the PP approximation is. The ratios between the exact and approximate results of the isotropy-breaking parts of the 2PCFs given in eq. (4.3),  $(2)\xi_{\lambda_1\lambda_2}^{X_1X_2}/(2)\xi_{\lambda_1\lambda_2\text{PP}}^{X_1X_2}$ , are plotted in the bottom panels. Basically, as  $\Theta$  increases, this ratio departs from unity, meaning that the error of the PP approximation becomes larger. In the  $\gamma\gamma$  case, for any  $\theta_d$ , the PP approximation works, at least, up to  $\Theta \sim 10^\circ$  because the error is within 10%. Similar but better results are obtained in the  $\delta\delta$  and  $uu$  cases (see figure 8). In contrast, the  $\delta\gamma$  case is sensitive to  $\theta_d$ , and if  $\theta_d = 45^\circ$ , the accuracy drops

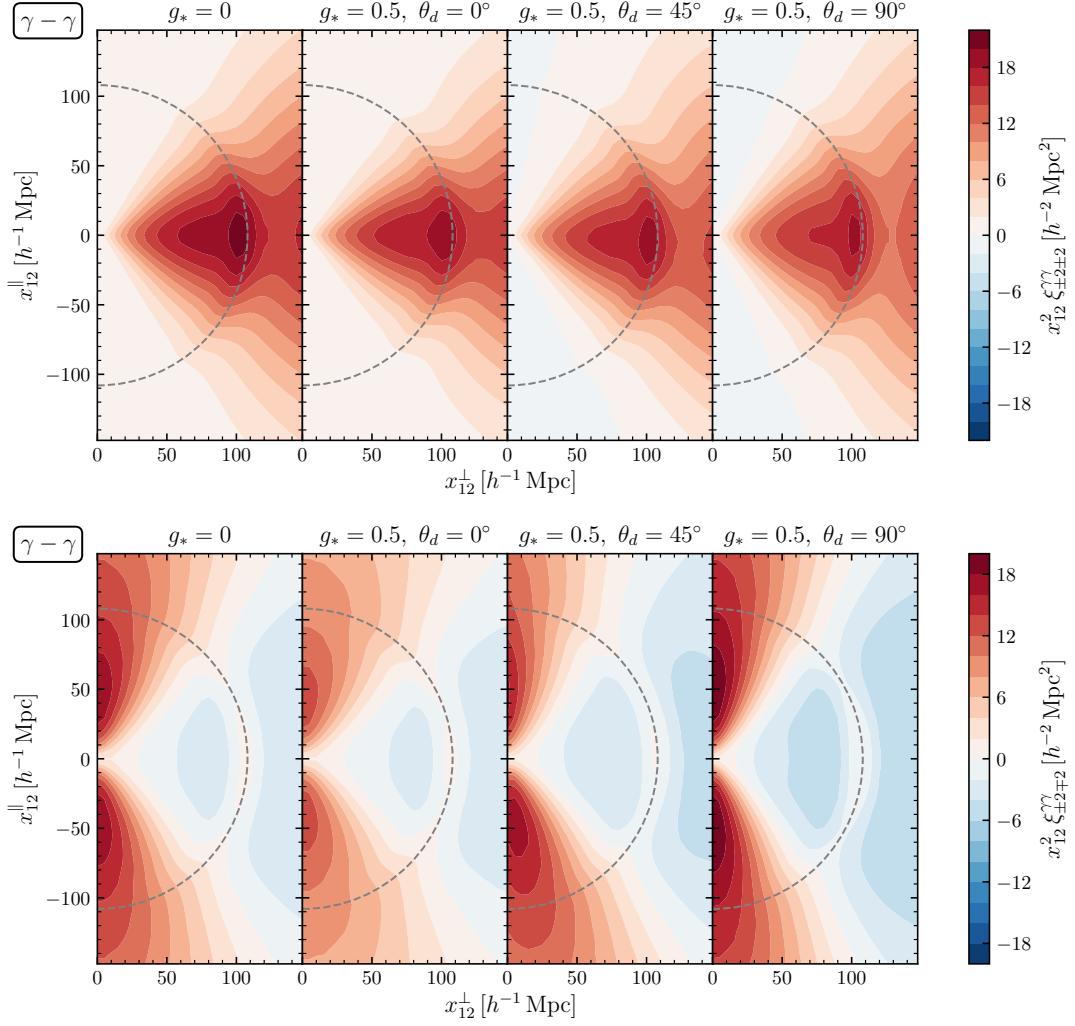


**Figure 5.** Same as figure 3, except for the  $\gamma\gamma$  correlation.

drastically and the error exceeds 10% already at  $\Theta \sim 4^\circ$ . For the  $u\gamma$  case, even worse, the PP approximation is totally spoiled. These indicate the importance of the analysis without the PP approximation for an accurate estimation of  $g_*$ . We note that, regarding the isotropic part  $^{(0)}\xi_{\lambda_1\lambda_2}^{X_1X_2}$ , for all the  $\delta\gamma$  and  $u\gamma$  and  $\gamma\gamma$  cases, the PP approximation works under  $\Theta \lesssim 30^\circ$  as shown in ref. [37].

## 5 Conclusions

In this paper, we have studied the impacts of the cosmic isotropy breaking on the 2PCFs of the galaxy intrinsic alignment or equivalently the spin-2 galaxy ellipticity field for the first time. To achieve this, we first have developed an efficient computation methodology of general types of the isotropy-breaking 2PCFs by generalizing the standard PolypoSH decomposition to the spin-weighted version. This is applicable to not only the analysis with the PP approximation but also the exact analysis.

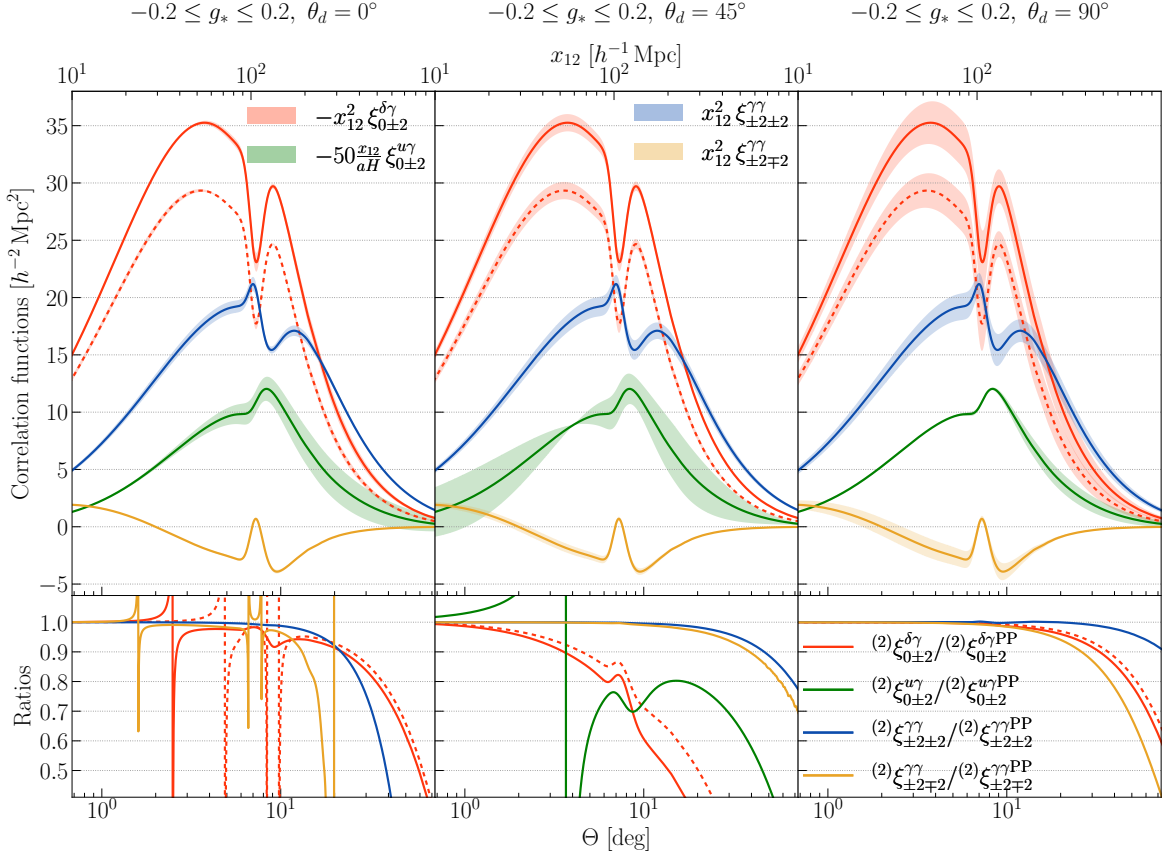


**Figure 6.** Absolute values of the 2PCFs  $\xi_{\lambda_1 \lambda_2}^{X_1 X_2}$  for  $-0.2 \leq g_* \leq 0.2$  (top panels) and ratios between the exact and PP-limit results of the isotropy-breaking parts  $^{(2)}\xi_{\lambda_1 \lambda_2}^{X_1 X_2}$  (bottom panels) for the  $\delta\gamma$ ,  $u\gamma$  and  $\gamma\gamma$  cases as a function of  $\Theta$  or  $x_{12}$  when  $z_1 = z_2 = 0.3$  and  $b_g = b_K = 1$ . Here, three different  $\hat{d}$ :  $\theta_d = 0^\circ$  (left panels),  $45^\circ$  (center panels) and  $90^\circ$  (right panels) are considered. In the top panels, the 2PCFs move under a range of  $g_*$  and are thus expressed with the finite-width lines (the central lines correspond to the results for  $g_* = 0$ ). Solid and dashed lines discriminate between the results in the redshift and real spaces, respectively. Note that all the results in the bottom panels are independent of  $g_*$ . In the bottom panels, some spiky features appear or some lines entirely disappear as  $^{(2)}\xi_{\lambda_1 \lambda_2}^{X_1 X_2}$  sometimes vanish.

As a concrete demonstration, we have analyzed the 2PCFs in a well-known  $g_*$  model according to this methodology. It has been confirmed that some isotropy-breaking distortions appear in the 2PCFs, and their shapes rely on a preferred direction causing the isotropy violation  $\hat{d}$ . Such a feature could be a distinctive indicator for testing the cosmic isotropy. Comparing between the exact and the PP-limit results, we have quantified the error of the PP approximation as a function of an opening angle between the LOS directions towards target galaxies  $\Theta$ . For the ellipticity auto correlation, the error exceeds 10% at  $\Theta \gtrsim 10^\circ$  for any  $\hat{d}$ . For the density-ellipticity and velocity-ellipticity cross correlations, the error is enhanced for specific  $\hat{d}$ , and the validity of the PP approximation is no longer guaranteed even at  $\Theta = \mathcal{O}(1^\circ)$ . This suggests the importance of the analysis beyond the PP approximation for an accurate isotropy test.

In the practical analysis, we have focused on the  $g_*$  model whose the matter power spec-

trum is given by eq. (4.1), predicting nonzero TripoSH monopole and quadrupole,  ${}_{\lambda_1\lambda_2}\Xi_{\ell\ell_1\ell_2\ell'}^{00X_1X_2}$  and  ${}_{\lambda_1\lambda_2}\Xi_{\ell\ell_1\ell_2\ell'}^{2MX_1X_2}$ . On the other hand, in other models that could yield nonzero higher multipoles  ${}_{\lambda_1\lambda_2}\Xi_{\ell\ell_1\ell_2\ell'}^{L>2, MX_1X_2}$  as mentioned in section 4, the 2PCFs would be distorted in a different fashion. Moreover, including contributions due to not only the matter distribution (scalar mode) but also the vorticity (vector mode) and the gravitational wave (tensor mode) [64, 69, 70] might yield other unique shapes in the 2PCFs. These could also be dealt with by our spin-weighted PolypoSH decomposition methodology owing to its high versatility, and should be studied in future works.

Our results have been obtained on the basis of the linear theory and hence might increase ambiguity at smaller scales. It should be checked with N-body simulations and the higher-order perturbation theory as done in ref. [71].

## Acknowledgments

M. S. is supported by JSPS KAKENHI Grant Nos. JP19K14718 and JP20H05859. T. O. acknowledges support from the Ministry of Science and Technology of Taiwan under Grant Nos. MOST 110-2112-M-001-045- and MOST 111-2112-M-001-061- and the Career Development Award, Academia Sinica (AS-CDA-108-M02) for the period of 2019 to 2023. K. A. is supported by JSPS Overseas Research Fellowships. M. S. and K. A. also acknowledge the Center for Computational Astrophysics, National Astronomical Observatory of Japan, for providing the computing resources of the Cray XC50.

## A Correlations of the density and velocity fields in the $g_*$ model

Here we summarize the same results as in section 4 but for the  $\delta\delta$ ,  $\delta u$  and  $uu$  cases.

Figure 7 describes the intensity distributions of the  $\delta\delta$ ,  $\delta u$  and  $uu$  correlations in the PP limit on the  $(x_{12}^\perp, x_{12}^\parallel)$  domain for nonzero  $g_*$  and several  $\theta_d$ . One can observe the distortions by nonzero  $g_*$  along the  $x_{12}^\perp$  axis, the diagonal line and the  $x_{12}^\parallel$  axis for  $\theta_d = 0^\circ$ ,  $45^\circ$  and  $90^\circ$ , respectively, similarly to the  $\delta\gamma$ ,  $u\gamma$  and  $\gamma\gamma$  cases.

Figure 8 depicts the  $\delta\delta$ ,  $\delta u$  and  $uu$  correlations and the ratios between the exact and PP-limit results of their isotropy-breaking parts as a function of  $x_{12}$  or  $\Theta$  for nonzero  $g_*$  and several  $\theta_d$ . The top panels indicate that the distortion level in the  $uu$ ,  $\delta u$  or  $\delta\delta$  correlation for a certain  $g_*$  varies depending on  $\theta_d$ , and is maximized for  $\theta_d \sim 0^\circ$ ,  $45^\circ$  or  $90^\circ$ . The bottom panels show that the PP approximation works independently of  $\theta_d$  when  $\Theta \lesssim 30^\circ$  for the  $\delta\delta$  and  $uu$  cases, while its validity is not guaranteed even when  $\Theta \sim 1^\circ$  for the  $\delta u$  case with  $\theta_d = 90^\circ$ .

## B Angular correlation functions

We here summarize the relation between the configuration-space correlations discussed in the main text and the angular correlations.

The spin- $|\lambda|$  field  ${}_\lambda X$  can be generally expanded with the spin-weighted spherical harmonics as

$${}_\lambda X(\mathbf{x}) = \sum_{\ell m} {}_\lambda a_{\ell m}^X {}_\lambda Y_{\ell m}(\hat{x}). \quad (\text{B.1})$$



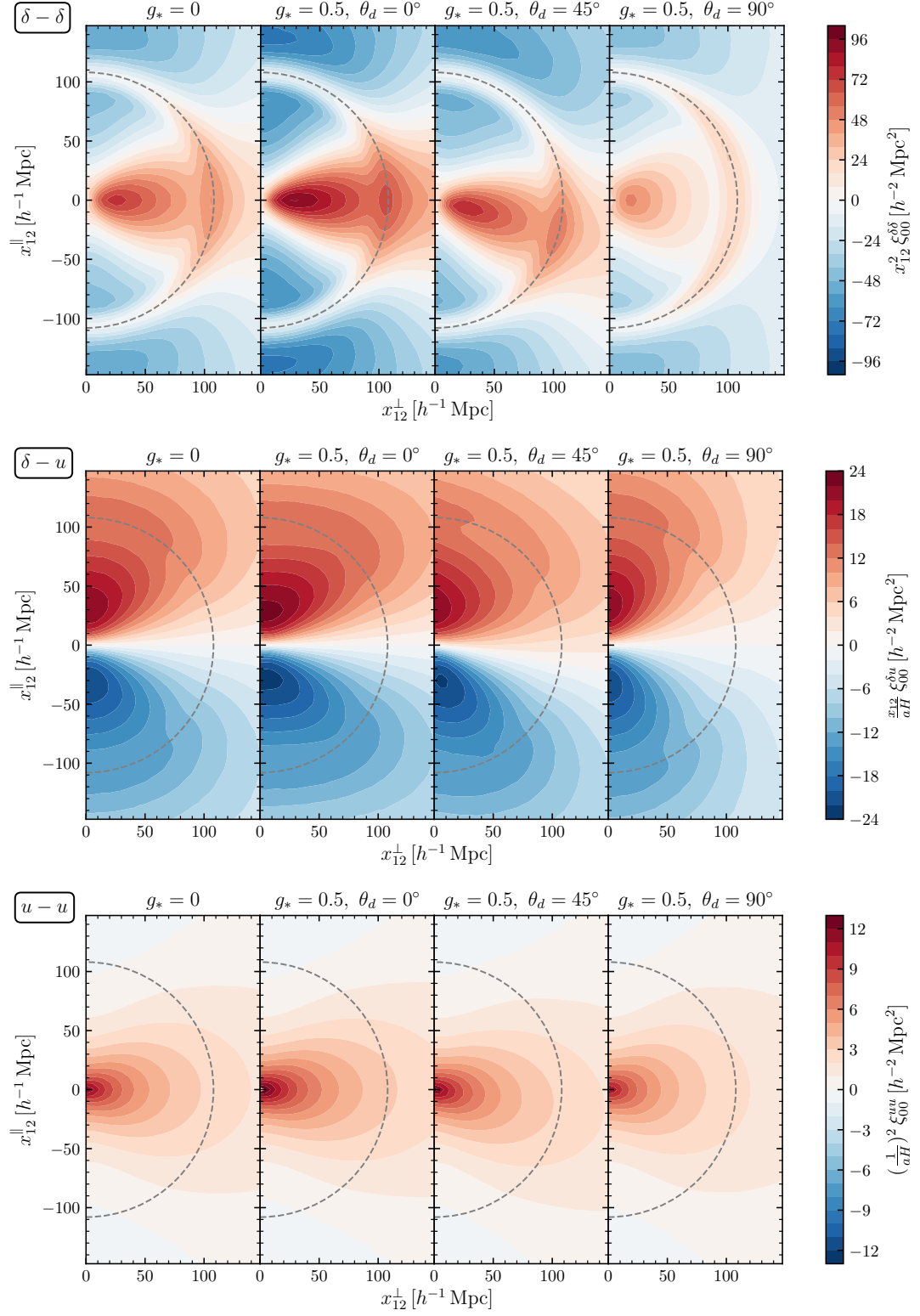


**Figure 7.** Same as figure 3, except for the  $\delta\delta$  and  $\delta u$  correlations in the redshift space and the  $uu$  one.



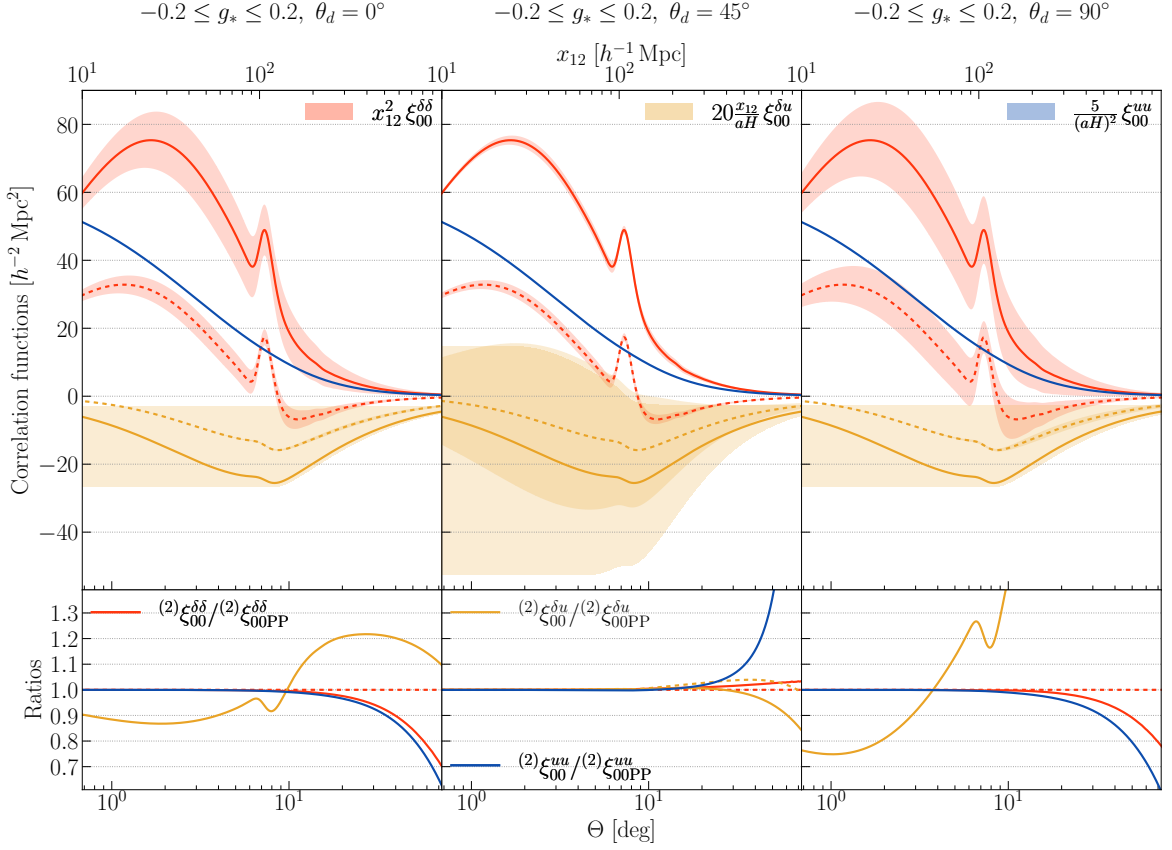


**Figure 8.** Same as figure 6, except for the  $\delta\delta$ ,  $\delta u$  and  $uu$  cases.

Employing eq. (2.8) and the identities in appendix C, the linear-theory form of the expansion coefficient is computed as

$$\begin{aligned} \lambda a_{\ell m}^X &= \int d^2 \hat{x} \lambda X(\mathbf{x})_\lambda Y_{\ell m}^*(\hat{x}) \\ &= 4\pi i^\ell \int \frac{d^3 k}{(2\pi)^3} Y_{\ell m}^*(\hat{k})_\lambda \mathcal{T}_\ell^X(k) \delta_m(\mathbf{k}), \end{aligned} \quad (\text{B.2})$$

where

$$\lambda \mathcal{T}_\ell^X(k) \equiv \sum_{jj'} \frac{4\pi i^{j-\ell} h_{jj'\ell}^{000} h_{jj'\ell}^{0\lambda-\lambda}}{(2\ell+1)(2j'+1)} c_{j'}^X(k) j_j(kx). \quad (\text{B.3})$$

Computing the correlation function of this  $\lambda a_{\ell m}^X$  by use of eqs. (3.2) and (C.4), we obtain

$$\langle \lambda_1 a_{\ell_1 m_1}^{X_1} \lambda_2 a_{\ell_2 m_2}^{X_2} \rangle = \sqrt{4\pi} i^{\ell_1-\ell_2} (-1)^{m_1+m_2} \sum_{LM} h_{\ell_1 \ell_2 L}^0 h_{\ell_1 \ell_2 L}^0 \begin{pmatrix} \ell_1 & \ell_2 & L \\ -m_1 & -m_2 & M \end{pmatrix} \lambda_1 \lambda_2 C_{\ell_1 \ell_2}^{LM X_1 X_2}, \quad (\text{B.4})$$

where

$$\lambda_1 \lambda_2 C_{\ell_1 \ell_2}^{LM X_1 X_2} \equiv \frac{2}{\pi} \int_0^\infty k^2 dk \lambda_1 \mathcal{T}_{\ell_1}^{X_1}(k) \lambda_2 \mathcal{T}_{\ell_2}^{X_2}(k) \bar{P}_m(k) \frac{G_{LM}(k)}{\sqrt{4\pi}}. \quad (\text{B.5})$$

Nonzero  $G_{L>0,M}$  generated from the isotropy-violating matter power spectrum induce nonzero off-diagonal modes  $\ell_1 \neq \ell_2$ . This is related to  $\xi_{\lambda_1\lambda_2}^{X_1X_2}$  as

$$\begin{aligned} \xi_{\lambda_1\lambda_2}^{X_1X_2}(\mathbf{x}_{12}, \hat{x}_1, \hat{x}_2) &= \sum_{\ell_1 m_1 \ell_2 m_2} \sqrt{4\pi} i^{\ell_1 - \ell_2} (-1)^{m_1 + m_2} \sum_{LM} h_{\ell_1 \ell_2 L}^0 \begin{pmatrix} \ell_1 & \ell_2 & L \\ -m_1 & -m_2 & M \end{pmatrix} \\ &\times \lambda_1 \lambda_2 C_{\ell_1 \ell_2}^{LM X_1 X_2} Y_{\ell_1 m_1}(\hat{x}_1) Y_{\ell_2 m_2}(\hat{x}_2). \end{aligned} \quad (\text{B.6})$$

In the PP limit, this is further simplified as

$$\begin{aligned} \xi_{\lambda_1\lambda_2\text{PP}}^{X_1X_2}(\mathbf{x}_{12}, \hat{x}_p) &= \sum_{\ell_1 \ell_2} \sqrt{4\pi} i^{\ell_1 - \ell_2} (-1)^{\lambda_1 + \lambda_2} \sum_{LM} \frac{h_{\ell_1 \ell_2 L}^0 h_{\ell_1 \ell_2 L}^{-\lambda_1 - \lambda_2}}{2L + 1} \\ &\times \lambda_1 \lambda_2 C_{\ell_1 \ell_2}^{LM X_1 X_2} Y_{L M}(\hat{x}_p). \end{aligned} \quad (\text{B.7})$$

For the derivation, we have used eqs. (C.4) and (C.5).

The harmonic coefficient of the spin-0 E/B-mode field is defined as<sup>4</sup>

$$\begin{aligned} {}_0a_{\ell m}^E &\equiv -\frac{1}{2} \left( +2a_{\ell m}^\gamma + -2a_{\ell m}^\gamma \right), \\ {}_0a_{\ell m}^B &\equiv -\frac{1}{2i} \left( +2a_{\ell m}^\gamma - -2a_{\ell m}^\gamma \right). \end{aligned} \quad (\text{B.8})$$

Because  $+2a_{\ell m}^\gamma = -2a_{\ell m}^\gamma$  and hence  ${}_0a_{\ell m}^E = -\pm 2a_{\ell m}^\gamma$  and  ${}_0a_{\ell m}^B = 0$ , the following relations hold:

$$\begin{aligned} \langle {}_0a_{\ell_1 m_1}^\delta {}_0a_{\ell_2 m_2}^E \rangle &= -\langle {}_0a_{\ell_1 m_1 \pm 2}^\gamma {}_0a_{\ell_2 m_2}^\gamma \rangle, \\ \langle {}_0a_{\ell_1 m_1}^u {}_0a_{\ell_2 m_2}^E \rangle &= -\langle {}_0a_{\ell_1 m_1 \pm 2}^u {}_0a_{\ell_2 m_2}^\gamma \rangle, \\ \langle {}_0a_{\ell_1 m_1}^E {}_0a_{\ell_2 m_2}^E \rangle &= \langle \pm 2a_{\ell_1 m_1}^\gamma \pm 2a_{\ell_2 m_2}^\gamma \rangle = \langle \pm 2a_{\ell_1 m_1}^\gamma \mp 2a_{\ell_2 m_2}^\gamma \rangle, \\ \langle {}_0a_{\ell_1 m_1}^\delta {}_0a_{\ell_2 m_2}^B \rangle &= \langle {}_0a_{\ell_1 m_1}^u {}_0a_{\ell_2 m_2}^B \rangle = \langle {}_0a_{\ell_1 m_1}^E {}_0a_{\ell_2 m_2}^B \rangle = \langle {}_0a_{\ell_1 m_1}^B {}_0a_{\ell_2 m_2}^B \rangle = 0. \end{aligned} \quad (\text{B.9})$$

## C Useful mathematical identities

The spherical harmonic decompositions: [48]

$$\begin{aligned} \mathcal{L}_l(\hat{k} \cdot \hat{x}) &= \frac{4\pi}{2l + 1} \sum_m Y_{lm}(\hat{k}) Y_{lm}^*(\hat{x}), \\ e^{i\mathbf{k} \cdot \mathbf{x}} &= \sum_{lm} 4\pi i^l j_l(kx) Y_{lm}(\hat{k}) Y_{lm}^*(\hat{x}), \\ \hat{k} &= \sum_m \boldsymbol{\alpha}^m Y_{1m}(\hat{k}) \\ \mathbf{m}_\pm(\hat{x}) &= \pm \sum_m \boldsymbol{\alpha}^m Y_{1m}(\hat{x}) \end{aligned} \quad (\text{C.1})$$

---

<sup>4</sup>See refs. [16, 70] for another convention that is different by sign from ours.

where a  $m$ -dependent vector  $\boldsymbol{\alpha}^m$ , given by

$$\boldsymbol{\alpha}^m \equiv \sqrt{\frac{2\pi}{3}} \begin{pmatrix} -m(\delta_{m,1}^K + \delta_{m,-1}^K) \\ i(\delta_{m,1}^K + \delta_{m,-1}^K) \\ \sqrt{2}\delta_{m,0}^K \end{pmatrix}, \quad (\text{C.2})$$

satisfies  $(\boldsymbol{\alpha}^m)^* = (-1)^m \boldsymbol{\alpha}^{-m}$  and

$$\boldsymbol{\alpha}^{m_1} \cdot \boldsymbol{\alpha}^{m_2} = \frac{4\pi}{3} (-1)^{m_1} \delta_{m_1, -m_2}^K. \quad (\text{C.3})$$

The addition theorem and the orthonormality of the spin-weighted spherical harmonics:

$$\begin{aligned} {}_{s_1}Y_{l_1 m_1}(\hat{n}) {}_{s_2}Y_{l_2 m_2}(\hat{n}) &= \sum_{s_3 l_3 m_3} {}_{s_3}Y_{l_3 m_3}^*(\hat{n}) h_{l_1 l_2 l_3}^{-s_1 - s_2 - s_3} \begin{pmatrix} l_1 & l_2 & l_3 \\ m_1 & m_2 & m_3 \end{pmatrix}, \\ \int d^2 \hat{n} {}_s Y_{l_1 m_1}(\hat{n}) {}_s Y_{l_2 m_2}^*(\hat{n}) &= \delta_{l_1, l_2}^K \delta_{m_1, m_2}^K. \end{aligned} \quad (\text{C.4})$$

The addition theorem of the Wigner symbols:

$$\sum_{m_1 m_2} \begin{pmatrix} l_1 & l_2 & l_3 \\ m_1 & m_2 & m_3 \end{pmatrix} \begin{pmatrix} l_1 & l_2 & l'_3 \\ m_1 & m_2 & m'_3 \end{pmatrix} = \frac{\delta_{l_3, l'_3}^K \delta_{m_3, m'_3}^K}{2l_3 + 1}. \quad (\text{C.5})$$

## References

- [1] E. Dimastrogiovanni, N. Bartolo, S. Matarrese and A. Riotto, *Non-Gaussianity and Statistical Anisotropy from Vector Field Populated Inflationary Models*, *Adv. Astron.* **2010** (2010) 752670, [[1001.4049](#)].
- [2] J. Soda, *Statistical Anisotropy from Anisotropic Inflation*, *Class. Quant. Grav.* **29** (2012) 083001, [[1201.6434](#)].
- [3] A. Maleknejad, M. Sheikh-Jabbari and J. Soda, *Gauge Fields and Inflation*, *Phys.Rept.* **528** (2013) 161–261, [[1212.2921](#)].
- [4] J. Beltran Jimenez and A. L. Maroto, *A cosmic vector for dark energy*, *Phys. Rev. D* **78** (2008) 063005, [[0801.1486](#)].
- [5] T. Hambye, *Hidden vector dark matter*, *JHEP* **01** (2009) 028, [[0811.0172](#)].
- [6] P. W. Graham, J. Mardon and S. Rajendran, *Vector Dark Matter from Inflationary Fluctuations*, *Phys. Rev. D* **93** (2016) 103520, [[1504.02102](#)].
- [7] M. Bastero-Gil, J. Santiago, L. Ubaldi and R. Vega-Morales, *Vector dark matter production at the end of inflation*, *JCAP* **04** (2019) 015, [[1810.07208](#)].
- [8] PLANCK collaboration, Y. Akrami et al., *Planck 2018 results. X. Constraints on inflation*, *Astron. Astrophys.* **641** (2020) A10, [[1807.06211](#)].
- [9] PLANCK collaboration, Y. Akrami et al., *Planck 2018 results. VII. Isotropy and Statistics of the CMB*, *Astron. Astrophys.* **641** (2020) A7, [[1906.02552](#)].
- [10] PLANCK collaboration, Y. Akrami et al., *Planck 2018 results. IX. Constraints on primordial non-Gaussianity*, *Astron. Astrophys.* **641** (2020) A9, [[1905.05697](#)].
- [11] A. R. Pullen and C. M. Hirata, *Non-detection of a statistically anisotropic power spectrum in large-scale structure*, *JCAP* **05** (2010) 027, [[1003.0673](#)].

- [12] N. S. Sugiyama, M. Shiraishi and T. Okumura, *Limits on statistical anisotropy from BOSS DR12 galaxies using bipolar spherical harmonics*, *Mon. Not. Roy. Astron. Soc.* **473** (2018) 2737–2752, [[1704.02868](#)].
- [13] N. E. Chisari and C. Dvorkin, *Cosmological Information in the Intrinsic Alignments of Luminous Red Galaxies*, *JCAP* **12** (2013) 029, [[1308.5972](#)].
- [14] F. Schmidt, N. E. Chisari and C. Dvorkin, *Imprint of inflation on galaxy shape correlations*, *JCAP* **10** (2015) 032, [[1506.02671](#)].
- [15] N. E. Chisari, C. Dvorkin, F. Schmidt and D. Spergel, *Multitracing Anisotropic Non-Gaussianity with Galaxy Shapes*, *Phys. Rev. D* **94** (2016) 123507, [[1607.05232](#)].
- [16] K. Kogai, T. Matsubara, A. J. Nishizawa and Y. Urakawa, *Intrinsic galaxy alignment from angular dependent primordial non-Gaussianity*, *JCAP* **08** (2018) 014, [[1804.06284](#)].
- [17] T. Okumura, A. Taruya and T. Nishimichi, *Intrinsic alignment statistics of density and velocity fields at large scales: Formulation, modeling and baryon acoustic oscillation features*, *Phys. Rev. D* **100** (2019) 103507, [[1907.00750](#)].
- [18] A. Taruya and T. Okumura, *Improving geometric and dynamical constraints on cosmology with intrinsic alignments of galaxies*, *Astrophys. J. Lett.* **891** (2020) L42, [[2001.05962](#)].
- [19] K. Kogai, K. Akitsu, F. Schmidt and Y. Urakawa, *Galaxy imaging surveys as spin-sensitive detector for cosmological colliders*, *JCAP* **03** (2021) 060, [[2009.05517](#)].
- [20] K. Akitsu, T. Kurita, T. Nishimichi, M. Takada and S. Tanaka, *Imprint of anisotropic primordial non-Gaussianity on halo intrinsic alignments in simulations*, *Phys. Rev. D* **103** (2021) 083508, [[2007.03670](#)].
- [21] T. Okumura and A. Taruya, *Tightening geometric and dynamical constraints on dark energy and gravity: Galaxy clustering, intrinsic alignment, and kinetic Sunyaev-Zel’dovich effect*, *Phys. Rev. D* **106** (2022) 043523, [[2110.11127](#)].
- [22] S. Saga, T. Okumura, A. Taruya and T. Inoue, *Relativistic distortions in galaxy density–ellipticity correlations: gravitational redshift and peculiar velocity effects*, *Mon. Not. Roy. Astron. Soc.* **518** (2023) 4976–4990, [[2207.03454](#)].
- [23] T. Okumura and A. Taruya, *First Constraints on Growth Rate from Redshift-Space Ellipticity Correlations of SDSS Galaxies at  $0.16 < z < 0.70$* , [[2301.06273](#)].
- [24] T. Kurita and M. Takada, *Constraints on anisotropic primordial non-Gaussianity from intrinsic alignments of SDSS-III BOSS galaxies*, [[2302.02925](#)].
- [25] Z. Vlah, N. E. Chisari and F. Schmidt, *An EFT description of galaxy intrinsic alignments*, *JCAP* **01** (2020) 025, [[1910.08085](#)].
- [26] Z. Vlah, N. E. Chisari and F. Schmidt, *Galaxy shape statistics in the effective field theory*, *JCAP* **05** (2021) 061, [[2012.04114](#)].
- [27] T. Matsubara, *The integrated perturbation theory for cosmological tensor fields I: Basic formulation*, [[2210.10435](#)].
- [28] T. Matsubara, *The integrated perturbation theory for cosmological tensor fields II: Loop corrections*, [[2210.11085](#)].
- [29] A. S. Szalay, T. Matsubara and S. D. Landy, *Redshift space distortions of the correlation function in wide angle galaxy surveys*, *Astrophys. J. Lett.* **498** (1998) L1, [[astro-ph/9712007](#)].
- [30] I. Szapudi, *Wide angle redshift distortions revisited*, *Astrophys. J.* **614** (2004) 51–55, [[astro-ph/0404477](#)].
- [31] J. Yoo and U. s. Seljak, *Wide Angle Effects in Future Galaxy Surveys*, *Mon. Not. Roy. Astron. Soc.* **447** (2015) 1789–1805, [[1308.1093](#)].

- [32] E. Castorina and M. White, *Beyond the plane-parallel approximation for redshift surveys*, *Mon. Not. Roy. Astron. Soc.* **476** (2018) 4403–4417, [[1709.09730](#)].
- [33] A. Taruya, S. Saga, M.-A. Breton, Y. Rasera and T. Fujita, *Wide-angle redshift-space distortions at quasi-linear scales: cross-correlation functions from Zel’dovich approximation*, *Mon. Not. Roy. Astron. Soc.* **491** (2020) 4162–4179, [[1908.03854](#)].
- [34] E. Castorina and M. White, *Wide angle effects for peculiar velocities*, *Mon. Not. Roy. Astron. Soc.* **499** (2020) 893–905, [[1911.08353](#)].
- [35] M. Shiraishi, T. Okumura, N. S. Sugiyama and K. Akitsu, *Minimum variance estimation of galaxy power spectrum in redshift space*, *Mon. Not. Roy. Astron. Soc.* **498** (2020) L77–L81, [[2005.03438](#)].
- [36] M. Shiraishi, K. Akitsu and T. Okumura, *Alcock-Paczynski effects on wide-angle galaxy statistics*, *Phys. Rev. D* **103** (2021) 123534, [[2103.08126](#)].
- [37] M. Shiraishi, A. Taruya, T. Okumura and K. Akitsu, *Wide-angle effects on galaxy ellipticity correlations*, *Mon. Not. Roy. Astron. Soc.* **503** (2021) L6–L10, [[2012.13290](#)].
- [38] M. Shiraishi, N. S. Sugiyama and T. Okumura, *Polypolar spherical harmonic decomposition of galaxy correlators in redshift space: Toward testing cosmic rotational symmetry*, *Phys. Rev. D* **95** (2017) 063508, [[1612.02645](#)].
- [39] N. Bartolo, A. Kehagias, M. Liguori, A. Riotto, M. Shiraishi and V. Tansella, *Detecting higher spin fields through statistical anisotropy in the CMB and galaxy power spectra*, *Phys. Rev. D* **97** (2018) 023503, [[1709.05695](#)].
- [40] K. Akitsu, N. S. Sugiyama and M. Shiraishi, *Super-sample tidal modes on the celestial sphere*, *Phys. Rev. D* **100** (2019) 103515, [[1907.10591](#)].
- [41] M. Shiraishi, T. Okumura and K. Akitsu, *Minimum variance estimation of statistical anisotropy via galaxy survey*, *JCAP* **03** (2021) 039, [[2009.04355](#)].
- [42] L. Ackerman, S. M. Carroll and M. B. Wise, *Imprints of a Primordial Preferred Direction on the Microwave Background*, *Phys. Rev. D* **75** (2007) 083502, [[astro-ph/0701357](#)].
- [43] T. Okumura and A. Taruya, *Anisotropies of galaxy ellipticity correlations in real and redshift space: angular dependence in linear tidal alignment model*, *Mon. Not. Roy. Astron. Soc.* **493** (2020) L124–L128, [[1912.04118](#)].
- [44] A. Hamilton, *Linear redshift distortions: A Review*, in *Ringberg Workshop on Large Scale Structure*, 8, 1997. [astro-ph/9708102](#). DOI.
- [45] T. Okumura, U. Seljak, Z. Vlah and V. Desjacques, *Peculiar velocities in redshift space: formalism, N-body simulations and perturbation theory*, *JCAP* **05** (2014) 003, [[1312.4214](#)].
- [46] P. Catelan, M. Kamionkowski and R. D. Blandford, *Intrinsic and extrinsic galaxy alignment*, *Mon. Not. Roy. Astron. Soc.* **320** (2001) L7–L13, [[astro-ph/0005470](#)].
- [47] C. M. Hirata and U. Seljak, *Intrinsic alignment-lensing interference as a contaminant of cosmic shear*, *Phys. Rev. D* **70** (2004) 063526, [[astro-ph/0406275](#)].
- [48] M. Shiraishi, D. Nitta, S. Yokoyama, K. Ichiki and K. Takahashi, *CMB Bispectrum from Primordial Scalar, Vector and Tensor non-Gaussianities*, *Prog. Theor. Phys.* **125** (2011) 795–813, [[1012.1079](#)].
- [49] M.-a. Watanabe, S. Kanno and J. Soda, *The Nature of Primordial Fluctuations from Anisotropic Inflation*, *Prog. Theor. Phys.* **123** (2010) 1041–1068, [[1003.0056](#)].
- [50] N. Bartolo, S. Matarrese, M. Peloso and A. Ricciardone, *Anisotropic power spectrum and bispectrum in the  $f(\phi)F^2$  mechanism*, *Phys. Rev. D* **87** (2013) 023504, [[1210.3257](#)].
- [51] J. Ohashi, J. Soda and S. Tsujikawa, *Observational signatures of anisotropic inflationary models*, *JCAP* **12** (2013) 009, [[1308.4488](#)].

- [52] N. Bartolo, S. Matarrese, M. Peloso and M. Shiraishi, *Parity-violating and anisotropic correlations in pseudoscalar inflation*, *JCAP* **1501** (2015) 027, [[1411.2521](#)].
- [53] A. Naruko, E. Komatsu and M. Yamaguchi, *Anisotropic inflation reexamined: upper bound on broken rotational invariance during inflation*, *JCAP* **04** (2015) 045, [[1411.5489](#)].
- [54] N. Bartolo, S. Matarrese, M. Peloso and M. Shiraishi, *Parity-violating CMB correlators with non-decaying statistical anisotropy*, *JCAP* **1507** (2015) 039, [[1505.02193](#)].
- [55] A. A. Abolhasani, M. Akhshik, R. Emami and H. Firouzjahi, *Primordial Statistical Anisotropies: The Effective Field Theory Approach*, *JCAP* **03** (2016) 020, [[1511.03218](#)].
- [56] T. Fujita, I. Obata, T. Tanaka and S. Yokoyama, *Statistically Anisotropic Tensor Modes from Inflation*, *JCAP* **07** (2018) 023, [[1801.02778](#)].
- [57] A. Kehagias and A. Riotto, *On the Inflationary Perturbations of Massive Higher-Spin Fields*, *JCAP* **07** (2017) 046, [[1705.05834](#)].
- [58] I. Obata and T. Fujita, *Footprint of Two-Form Field: Statistical Anisotropy in Primordial Gravitational Waves*, *Phys. Rev. D* **99** (2019) 023513, [[1808.00548](#)].
- [59] N. Bartolo, S. Matarrese, M. Peloso and A. Ricciardone, *Anisotropy in solid inflation*, *JCAP* **1308** (2013) 022, [[1306.4160](#)].
- [60] N. Bartolo, M. Peloso, A. Ricciardone and C. Unal, *The expected anisotropy in solid inflation*, *JCAP* **1411** (2014) 009, [[1407.8053](#)].
- [61] K. W. Masui and U.-L. Pen, *Primordial gravity wave fossils and their use in testing inflation*, *Phys. Rev. Lett.* **105** (2010) 161302, [[1006.4181](#)].
- [62] L. Dai, D. Jeong and M. Kamionkowski, *Anisotropic imprint of long-wavelength tensor perturbations on cosmic structure*, *Phys. Rev. D* **88** (2013) 043507, [[1306.3985](#)].
- [63] F. Schmidt, E. Pajer and M. Zaldarriaga, *Large-Scale Structure and Gravitational Waves III: Tidal Effects*, *Phys. Rev. D* **89** (2014) 083507, [[1312.5616](#)].
- [64] K. Akitsu, Y. Li and T. Okumura, *Gravitational wave fossils in nonlinear regime: halo tidal bias and intrinsic alignments from gravitational wave separate universe simulations*, [2209.06226](#).
- [65] K. Akitsu, M. Takada and Y. Li, *Large-scale tidal effect on redshift-space power spectrum in a finite-volume survey*, *Phys. Rev. D* **95** (2017) 083522, [[1611.04723](#)].
- [66] K. Akitsu and M. Takada, *Impact of large-scale tides on cosmological distortions via redshift-space power spectrum*, *Phys. Rev. D* **97** (2018) 063527, [[1711.00012](#)].
- [67] Y. Li, M. Schmittfull and U. s. Seljak, *Galaxy power-spectrum responses and redshift-space super-sample effect*, *JCAP* **02** (2018) 022, [[1711.00018](#)].
- [68] C.-T. Chiang and A. z. Slosar, *Power spectrum in the presence of large-scale overdensity and tidal fields: breaking azimuthal symmetry*, *JCAP* **07** (2018) 049, [[1804.02753](#)].
- [69] F. Schmidt and D. Jeong, *Cosmic Rulers*, *Phys. Rev. D* **86** (2012) 083527, [[1204.3625](#)].
- [70] M. Biagetti and G. Orlando, *Primordial Gravitational Waves from Galaxy Intrinsic Alignments*, *JCAP* **07** (2020) 005, [[2001.05930](#)].
- [71] T. Okumura, A. Taruya and T. Nishimichi, *Testing tidal alignment models for anisotropic correlations of halo ellipticities with N-body simulations*, *Mon. Not. Roy. Astron. Soc.* **494** (2020) 694–702, [[2001.05302](#)].